UNIVERSITY OF OKLAHOMA

GRADUATE COLLEGE

TECHNIQUES FOR SIMULTANEOUS TRANSMIT AND RECEIVE WITH ALL-DIGITAL ARRAYS

A THESIS

SUBMITTED TO THE GRADUATE FACULTY

in partial fulfillment of the requirements for the

Degree of

MASTER OF SCIENCE

By

HEATH VANN
Norman, Oklahoma
2021

TECHNIQUES FOR SIMULTANEOUS TRANSMIT AND RECEIVE WITH ALL-DIGITAL ARRAYS

A THESIS APPROVED FOR THE
SCHOOL OF ELECTRICAL AND COMPUTER ENGINEERING

BY THE COMMITTEE CONSISTING OF

Dr. Nathan Goodman, Chair

Dr. Caleb Fulton

Dr. Justin Metcalf

Table of Contents

Table of Contents iv

List of Tables vi

List of Figures vii

Abstract xi

1 Introduction 1

1.1 Thesis Outline 2

2 Digital Array Configuration 4

2.1 Signal Model 5

2.2 Subarray Configurations 7

2.3 Array Environment 12

2.4 Pulse Modeling 14

2.5 Transmitter and Receiver Noise 17

2.6 Quadrature Amplitude Modulation 18

3 Mutual Coupling Analysis 21

3.1 Theory 22

3.2 Estimation of Scattering Parameters 25

3.3 Application 31

3.4 Array Impact 32

4 Adaptive Beamforming **37**

4.1 Theory 38

4.2 Adaptive Transmit Beamformer 39

4.3 Impact on Transmit Subarray 42

4.4 Impact on Receive Subarray 45

4.5 Sensitivity to Mutual Coupling Estimation 50

4.6 Transmitted Beam Position Impact 52

4.7 Adaptive Receive Beamformer 53

4.8 Comparison 54

5 Digital Cancellation **57**

5.1 Theory 58

5.2 System Setup 62

5.3 Performance 64

5.4 Impact of Filter Order 67

5.5 Impact of Transmitter Noise 69

5.6 Sensitivity to Mutual Coupling Estimation 71

6 Results **73**

6.1 Simulation Setup 73

6.2 Adaptive Beamforming 74

6.3 Digital Cancellation 75

6.4 Total 79

7 Conclusion & Future Work **84**

References **86**

List of Tables

4.1 Comparison of different transmit beamforming schemes 43

List of Figures

2.1 Digital array configuration and corresponding beam pattern(s), normalized to peak gain achievable by utilizing full aperture. 10
2.2 Digital array configuration and corresponding beam pattern(s), normalized to peak gain achievable by utilizing full aperture. 10
2.3 Digital array configuration and corresponding beam pattern(s), normalized to peak gain achievable by utilizing full aperture. 10
2.4 Digital Array Environment for Multi-Function Operation 13
2.5 Windowed Linear-Frequency-Modulated radar pulse with a pulse with of 1 microsecond and a bandwidth of 100 MHz. 16
2.6 Transmitted LFM Spectrum for each element on 1 row of the transmitting subarray 17
2.7 Transmitted 16-QAM signal used to measure multi-function performance in the time domain (left) and the symbol constellations (right) 20

3.1 Visual representation of mutual coupling between antenna elements in an array 23
3.2 Scattering parameters of a 256 element dipole array 29
3.3 Scattering parameters for a singular element in a 256 element dipole array 30

3.4 Application of coupling coefficients in the frequency domain. Total leakage signal is the combination of distorted pulses from all transmitting elements. 33
3.5 Average leakage power for each element in the receive subarray. Adjacent columns to the transmitter are marked for clarity. 34

4.1 Mean-squared leakage power as a function of adaptive iterations . . 42
4.2 Array radiation patterns utilizing the adaptive beamforming weights normal to the array (left) and steered off-axis (right). The array was split into side-by-side horizontal subarrays, corresponding to the azimuth principle plane. 45
4.3 Comparison of the number of saturated elements for different transmit beamforming schemes 47
4.4 Comparison of average leakage power per receiver element under different beamforming schemes 48
4.5 Power maps of 3 different transmit beamforming schemes: uniformly weighted (top), 1-column guard (middle), and adaptive (bottom). The array was transmitting on the left half of the array, with incident leakage on the right half. 49
4.6 Average leakage power as a function of S-matrix uncertainties utilizing both uniform and adaptive beamforming weights 51
4.7 Calculated leakage power for various transmitted beam positions. Calculated with both uniform (left) and adaptive (right) transmit beamforming weights. 52
4.8 Isolation under different beamforming schemes. Transmit power is defined as power per element 55

5.1 System setup utilizing complete reconstruction of $\mathbf{S}$ and an ideal input 63

5.2 System setup utilizing complete reconstruction of $\mathbf{S}$ and a measured input for each transmitting element 64
5.3 System setup utilizing a single FIR filter and a priming signal $y_{int}(t)$ 65
5.4 Transmitted interference signal and filtered signal 66
5.5 Beamformed receiver spectrum without (left) and with (right) digital cancellation 66
5.6 Residue power after digital cancellation versus filter order for different time-bandwidth products 68
5.7 Residue power after digital cancellation as a function of transmitter noise level for each of the three proposed techniques. The single FIR filter technique is denoted as FIR filter, while the other techniques are denoted with respect to the system inputs. 70
5.8 Residue power as a function of uncertainties in the S-matrix 72

6.1 Dynamic range of receiver elements with incident leakage signal, without (left) and with (right) adaptive beamforming. Blue regions indicate the original dynamic range of the receiver, and the red regions indicate the leakage signal levels. 75
6.2 Constellation diagrams of beamformed receive signal with (right) and without (left) added digital cancellation signal. The view of the right diagram was zoomed in to highlight the difference in symbol variance during and after radar pulse transmission 76
6.3 Eye diagrams of beamformed 4-QAM signal under differing levels of transmitter noise. Plotted during and after transmitted radar pulse. 78
6.4 Bit-error rates for different transmit beamforming schemes and transmitter power levels 80
6.5 Subarray isolation provided by STAR algorithms. Dotted lines indicate digital cancellation of the transmitted leakage signals 82

6.6 Bit-error rates of the external signal provided by STAR algorithms. Dotted lines indicate digital cancellation of the transmitted leakage signals. Signal power is referenced from transmitting antenna 10 km from array. 83

Abstract

The increased flexibility provided by all-digital array architectures allows for the development of improved techniques toward achieving multi-function capability. In an all-digital array, element-level control can be utilized to create a variety of subarray configurations that can be operated independently to form multiple simultaneous transmit and receive (STAR) beams. This thesis describes how STAR can be implemented on an all-digital array by partitioning the array into subarrays, and details various techniques to improve the STAR performance by increasing the isolation between subarrays. A metric to quantify subarray isolation is provided, which incorporates both transmit/receive gain and the leakage power produced by mutual coupling between subarrays.

The strategies used to increase subarray isolation leverage knowledge of the scattering parameters of the array, which describe the mutual coupling between subarrays. By formulating the leakage power between subarrays in terms of the scattering parameters of the array, adaptive beamformers can be designed on both transmit and receive to minimize the incident leakage and increase subarray isolation. Digital cancellation of the leakage signals can be used to further increase subarray isolation, with an estimate of the leakage signal provided by the scattering parameters. The proposed techniques for STAR provide insight into the multi-function capability afforded by all-digital arrays, and may become more sophisticated as the use of all-digital arrays becomes ubiquitous.

Chapter 1

Introduction

Phased array antenna systems have been heavily utilized in communication and defense systems for many years [1]-[2]. Recent advances in FPGA technology and analog-to-digital converters have pushed all-digital arrays to the forefront of research and design due to the increased flexibility and control provided by element-level digitization [3]. One exciting area of flexibility provided by digital arrays is the advancement of aperture-level simultaneous transmit and receive (STAR) configurations. Digital arrays allow for dynamic aperture reconfiguration, which can be utilized to define separate transmit/receive subarrays tailored for specific applications [4]. Due to the close proximity between adjacent subarrays, the transmission of high-power signals from one subarray will leak onto adjacent subarrays, lowering the subarray isolation and SINR. Therefore, the fundamental limit of STAR systems is the amount of isolation provided between transmit/receive chains, which determines the dynamic range capable by the receiver [5]. This thesis describes how a digital array can be utilized for aperture-level STAR, and investigates different techniques used to increase the isolation between subarrays.

Control over the amplitude and phase of individual radiating elements in a phased array allows for electronic steering and beamshape control. Digital beamformers have been studied in the past for a variety of applications in multiple-input-

multiple-output (MIMO) systems, as they allow for adjustable gain between multiple incoming/outgoing signals [6]. Adaptive beamforming schemes have been utilized in radar systems to minimize interference from external sources [7] such as unwanted reflections or jamming signals. Because aperture-level STAR arrays suffer reduced SINR from leakage signals between subarrays, this thesis examines how adaptive digital beamforming techniques can be implemented to minimize the self-interference between subarrays.

Self-interference describes the impact of the transmitted signals from the array onto itself. Cancellation techniques for self-interference have been well explored in the past at both the analog and digital level [8]-[9], particularly in MIMO communications systems [10]. Self-interference caused by transmitted radar signals in an aperture-level STAR array provides new avenues of utilizing self-interference cancellation algorithms. This thesis examines the impact and limitations of digital cancellation of self-interference from transmitted radar waveforms on an all-digital array.

1.1 Thesis Outline

The remaining chapters of this thesis are organized as follows. Chapter 2 details the fundamentals behind digital array processing and how it relates to multifunction applications. Specifically, the signal models of the transmitted/received signals are described in detail along with the corresponding imperfections. Also included are the subarray configurations required for STAR.

Chapter 3 gives a brief introduction to mutual coupling in arrays, outlines a technique that can be used to estimate the mutual coupling parameters, and explains the impact mutual coupling will have toward achieving STAR capabilities.

Chapter 4 describes how adaptive beamforming techniques can be used to reduce the leakage power between subarrays and thereby increase the subarray isolation. The impact of the beamformers on the transmit/receive beams and gain is also discussed.

Chapter 5 introduces digital cancellation of the transmitted leakage signal, which can be used to further increase subarray isolation. The sensitivity and limitations of the digital cancellation algorithm are also covered, as well as comparisons between digital cancellation algorithms.

Chapter 6 overviews the performance of the digital array simulation in achieving STAR. This is measured by the ability of the array to decode external communication signals during periods of radar transmission. The impact of the adaptive beamforming and digital cancellation algorithms are also compared and used in tandem.

Chapter 7 concludes the thesis and provides areas of potential further research into STAR with digital arrays.

Chapter 2

Digital Array Configuration

All-digital arrays have been considered the next big leap in phased array antennas for many years. Benefits of digital array architecture are discussed throughout the literature [11], with common themes including the increase in flexibility and beamforming capabilities provided by element-level control. One exciting area of flexibility provided by digital arrays is the ability to partition the array into multiple simultaneously functioning subarrays, and achieving aperture-level simultaneous transmit and receive (STAR). Partitioning of the array is accomplished by the element-level control of the individual radiating elements, which can be excited in ways to produce multiple simultaneous beams. In order to examine techniques for simultaneous transmit and receive on a digital array, it is important to first cover the foundation of all-digital array architecture and signal processing. A MATLAB simulation can be developed to model aspects of all-digital array architecture and signal processing, and provides a good framework to develop techniques for STAR on a partitioned array. This chapter begins with the fundamentals of digital array processing, and details how properties of the array are simulated to begin algorithm development for STAR functionality.

2.1 Signal Model

The distinctive feature of digital phased array antennas, as the name suggests, is the ability to transmit and receive independent IQ streams from each element of the array. Whereas previous phased array systems were limited to independent IQ streams on subarrays comprised of multiple elements, digital arrays allow for complete control of every individual element in the array. This element-level control provides increased beamforming capabilities and flexibility on the number of transmitted/received beams. In order to get a better understanding of how the individual elements in the array collimate together to produce coherent beams, it is first necessary to look at the signal model for a single element. In an N-element array, let $a_n(t)$ denote the signal transmitted from the nth element in the array. Then

$$a_n(t) = \alpha_n(t)e^{j(\omega t+\theta_n(t))} \tag{2.1}$$

where $\alpha_n(t)e^{\theta_n(t)}$ comprises the complex envelope of the transmitted pulse for the nth element in the array. The complex envelope of the transmitted pulse is where the information on the signal is stored, as the high RF carrier ω is downconverted in the receiver hardware. The total transmitted signal from the array is then given by the sum of all the individual transmitted waveforms in the far field of the array, according to

$$a_{TX}(t) = \sum_{n=1}^{N} a_n(t)e^{-j\vec{K}\cdot\vec{r}_n}. \tag{2.2}$$

In the far field of the array, the differences in the complex envelopes $\theta_n(t)$ and signal amplitudes $\alpha_n(t)$ produced by the elements' positional differences will be minimal, so that $\alpha_n(t)e^{j\theta_n(t)} \approx \alpha(t)e^{j\theta(t)}$ for all transmitted signals in the array.

As the signals propagate through space, the oscillation of the carrier frequency is described in three dimensions by the wavenumber $\vec{K}$ given by

$$\vec{K} = \frac{2\pi}{\lambda}\vec{u} = K_x\vec{u}_x + K_y\vec{u}_y + K_z\vec{u}_z \tag{2.3}$$

where $\vec{u}$ is a unit vector in the propagation direction and λ is the wavelength of the carrier frequency. At any particular direction $\vec{K}$, the transmitted signal can be described by

$$a_{TX}(t, \vec{K}) = a(t)\sum_{n=1}^{N} e^{-j\vec{K}\cdot\vec{r}_n} \tag{2.4}$$

where $\vec{r}_n$ is the vector defining the location of the nth antenna element. If all of the elements are excited with constant phase (and assuming a planar array), the peak directivity of the array will be found normal to the array face. (2.4) above shows that the total signal in the far field is the sum of complex weights due to the transmitted signal multiplied by a phase shift depending on the element's position. Because these phase shifts are known, they can be exploited to steer the transmitted beam in space.

As mentioned above, another benefit of phased arrays is the ability to electronically scan the transmitted beam(s) by producing a constant phase front of the transmitted signals in a particular direction in space. In order to collimate a transmit beam in the direction given by $\vec{K}_{TX}$, a transmit beamformer $\mathbf{w_{TX}}$ can be designed to align the transmitted phase of each element's signal in the far-field at the direction specified by $\vec{K}_{TX}$. Define the transmit beamformer weight on the nth element as

$$w_{TX}[n] = A_n e^{j\vec{K}_{TX}\cdot\vec{r}_n} \tag{2.5}$$

so that the total transmitted signal is given in the far-field as

$$a_{TX}(t) = a(t) \sum_{n=1}^{N} A_n e^{-j(\vec{K}-\vec{K}_{TX})\cdot\vec{r}_n}. \tag{2.6}$$

Clearly, the signal is maximized at the location where $\vec{K}$ matches $\vec{K}_{TX}$. The phase shift required on each individual element is therefore given by $\vec{K}_{TX} \cdot \vec{r_n}$. Because of the digital architecture, the waveforms and phase shifts can be applied independently to every element, allowing for an abundance of beamforming schemes. The amplitude of the beamforming weights A_n can be used to control the shape of the transmitted beam, producing lower sidelobe levels and/or broadening the main beamwidth..

Similar to the transmit beamformer, a receive beamformer can be applied on receive to focus the direction of receive beam(s) to the desired locations $\vec{K}_{RX}$. Receive beamforming is done in exactly the same manner as in the transmit case, with $\mathbf{w_{RX}}$ signifying the receive beamforming weights. One useful property of all-digital arrays is the ability to form multiple simultaneous receive beams. Because the received signal on each element is digitized, the stored element-wise IQ data can be passed through multiple different digital beamformers to form multiple receive beams. These simultaneous receive beams can be used to drastically reduce the scanning time of a region in space, or to perform fine angle estimations of a target [12]. With the production of multiple simultaneous beams, digital arrays lend themselves well for multi-function capability.

2.2 Subarray Configurations

Multi-function arrays must be able to separate functionality in time, frequency, or space. If multiple functions will be utilized at simultaneous time periods, the array must possess some form of STAR capability to process multiple transmit and

receive beams simultaneously. In this study, STAR was implemented by creating separate partitions of the array elements for separate functions (transmit/receive). Each of these partitions, or subarrays, consist of the combination of signals transmitted/received from all of the individual elements in that subarray. Therefore, each subarray will generate its own beam in space and allows the array to complete multiple functions at once. Again, because every element is digitized, beams can be created from any combination of elements. These partitions lead to another advantage of all-digital arrays: the ability to form arbitrary subarrays from scan to scan.

The advantages provided by subarrays can be explained in terms of the transmitted/received beams. Each subarray on transmit can provide a separate radiated beam in space, which can be steered in separate directions as desired. As mentioned in Section 2.1, multiple receive beams can be formed simultaneously from any combination of elements. In other words, receive beams are not limited in number to the number of particular subarrays, but can be formed using the entire array for multiple directions at once. While forming multiple receive beams does increase computation, it can be beneficial in many applications. In this study, because the focus was on multi-function arrays, receive beams were limited to the defined receive subarray partitions. Although this limits the array gain due to the decrease in receiving elements, limiting the receive beams to their defined subarrays allows for other subarrays to be transmitting while the receive subarray is focused on an external target. This study does not allow for any individual element to be both transmitting and receiving at a single instant in time, although study has been done in this area in the past [13]. The case where all other subarrays are transmitting while one subarray is receiving would be the baseline performance, and as such is the highlight of this study. However, increased receiver gain could be obtained dur-

ing time periods in between pulses by utilizing all elements in the array for receive beamforming.

The radiation pattern provided by summing up the signals from separate elements is known as the array factor. The array factor is typically calculated for all angles in space, and describes the radiation intensity of the combined signals in the far-field of the array. While the array factor provides a good approximation of the transmitted beam, it does not encapsulate the radiation of the individual array antenna elements. Each individual element in the array will have its own radiation characteristics, which will affect how the radiated signals are combined in space. In large arrays, the element radiation patterns are generally consistent for most elements in the array, with deviations found toward the array edges. Further analysis of the radiation characteristics of the array is discussed in Chapter 3. For now, the radiated field of the array can be derived using the product of the element radiation pattern, assumed the same for all elements, and the array factor. A common element pattern used for array analysis is a raised cosine, with a peak gain normal to the array face. These expressions for radiation patterns can be used to describe the radiation characteristics of different subarray configurations.

There are an abundance of different subarray configurations that can be implemented on a digital array. Different subarray configurations will produce differing array factors in the far field, and combinations of beamforming techniques allow for increased multi-function flexibility. Fundamentally, partitioning the array will produce a reduction in gain and an increase in beamwidth along a particular principle plane. The simplest realizations of subarray configurations are examined in this research, although adaptive methods of subarray selection have been studied in previous work [4]. Figure 2.1 shows the full aperture subarray configuration and cut of the corresponding beam pattern, where all elements in the array are collimated

into one beam. Partition-based STAR is impossible in this configuration, as all

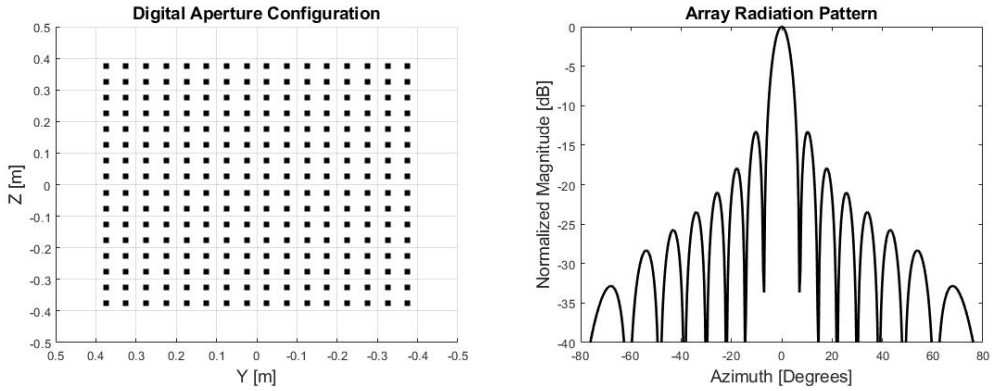

Figure 2.1: Digital array configuration and corresponding beam pattern(s), normalized to peak gain achievable by utilizing full aperture.

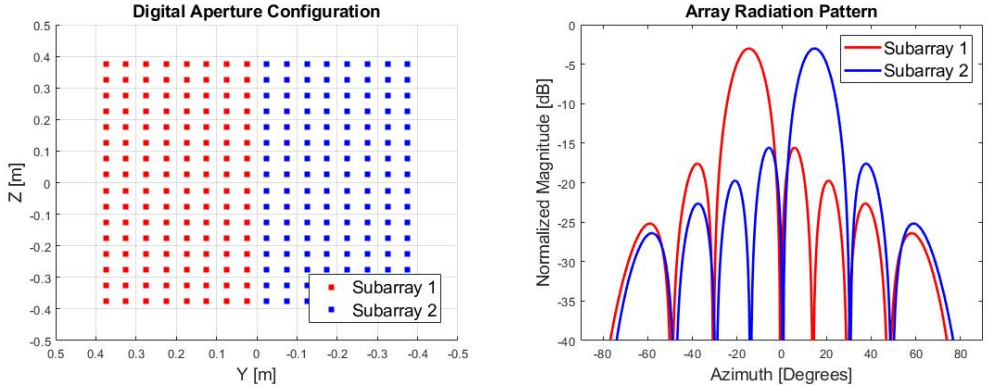

Figure 2.2: Digital array configuration and corresponding beam pattern(s), normalized to peak gain achievable by utilizing full aperture.

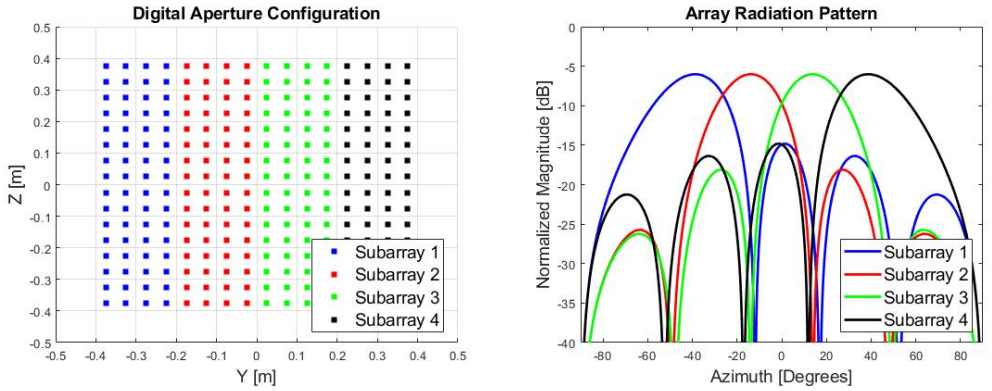

Figure 2.3: Digital array configuration and corresponding beam pattern(s), normalized to peak gain achievable by utilizing full aperture.

elements would have to be transmitting simultaneously to focus a single beam with maximum gain. However, this configuration maximizes the array gain for a particular beam, and produces the minimum 3-dB beamwidth possible by the array in both principal planes. For planar arrays, the 3-dB beamwidth can be approximated as:

$$\theta_{3dB} = 0.886\frac{\lambda}{L} \tag{2.7}$$

where L is the length of the array along the principal plane. Therefore a separate beamwidth is generated in each principal plane, depending on the aperture length along that principal plane. For a 16x16 array at half-wavelength spacing, the 3-dB beamwidth is approximately 6.35 degrees. Figure 2.2 shows a configuration where the array is split into equally sized subarrays. In this subarray configuration, two beams are formed simultaneously and independently steered from each subarray. In a STAR scenario, one subarray would be transmitting pulses (presumably for radar) while the other subarray receives signals. These received signals could be reflections from the transmitted radar pulses, or some other external signal of interest. Mutual coupling between the two subarrays would also be present, and poses many issues for receiver performance (discussed in Chapter 3). Looking at the transmitted patterns for each subarray in Figure 2.2, it is also evident that the 3-dB beamwidth of the two beams is larger (12.69 degrees) than that of the full aperture configuration along the azimuth axis. This beam broadening is caused by the reduced aperture length along the Y dimension. The 3-dB beamwidth in the elevation principal plane would still remain at 6.35 degrees. Also, because only half of the array is transmitting for each beam, the peak gain of each of the beams is reduced by half as well.

Figure 2.3 shows a configuration where the array is divided into four equally sized subarrays. Just as in the case with two subarrays, each of the four subar-

rays could have its own individual waveform, and the focused beams are much wider (25.38 degrees) and have one-fourth of the peak gain of the full array. While this configuration would certainly add complexity to the system, the techniques to enable STAR functionality with all subarrays would function largely the same regardless of the number of subarrays. Still, any partitioning of the aperture would produce increased beamwidth and reduced gain for each subarray beam compared to the full aperture beam. The increase in the number of beams, however, enables STAR and allows for multi-function capability.

2.3 Array Environment

Now that the signal model and subarray configurations have been described for a STAR array, a simplified block diagram can be created to model the array environment that will be of interest in this work. Figure 2.4 shows a simplified block diagram of a typical all-digital array, split into transmit and receive subarrays.

First, it is important to note how each individual element is connected directly to the digital backend, as opposed to being combined together in subarray blocks. This architecture is the foundation of all-digital arrays, as the digital control over each antenna element provides improved flexibility and control over the array signals. Also, the block diagram gives a clear representation of the subarray functions described in Section 2.2. Specifically, the transmit subarray is transmitting radar pulses, while the receive subarray is focused on receiving the external communications signal. Ideally, the two subarrays would operate independently from one another with high levels of isolation, while still being capable of combining the signals together when utilizing the full aperture for a single receive beam. However, because of the close proximity between the two subarrays on the same aperture, mu-

tual coupling between antenna elements will hinder the subarray isolation. These mutual coupling effects are examined more closely in Chapter 3, as the mutually coupled radar pulses will be the biggest obstacle to STAR operation.

Another aspect of the block diagram is the transmit/receive (T/R) modules. Each T/R module would contain the hardware necessary to mix the digital baseband signal up to the RF carrier, amplify the signal, and propagate into space, with a separate chain used to receive the RF signal, amplify, and mix back to baseband. The T/R modules will therefore include some form of digital-to-analog converter and high-power amplification on each element. On receive, each element contains an adjustable low-noise amplifier and analog-to-digital converter. Also included in the T/R modules are necessary filters set to encompass the transmitted/received sig-

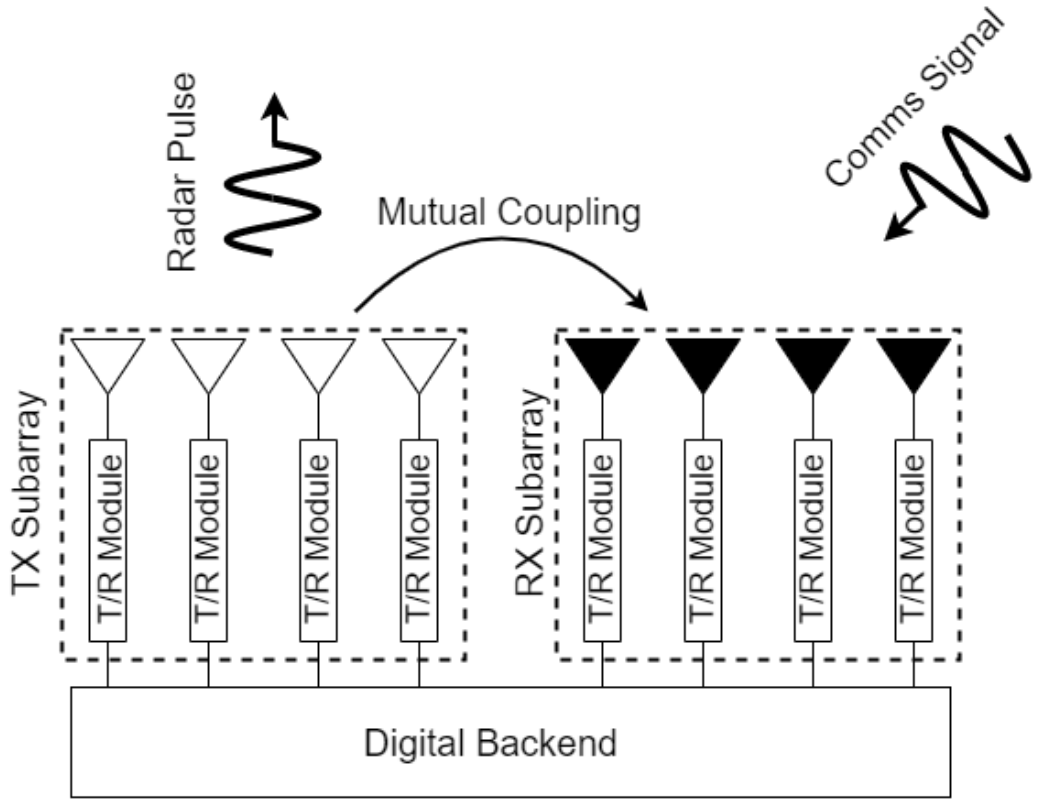

Figure 2.4: Digital Array Environment for Multi-Function Operation

nal spectra. Between the T/R modules and the antenna elements, typically arrays utilize circulators or switches to control the flow of data between transmitting and receiving. While the performance of the circulators were assumed ideal, overall the T/R modules will be modeled with random differences to allow for hardware imperfections.

2.4 Pulse Modeling

A typical radar system transmits a train of pulses into the atmosphere to measure reflections off of scatterers. Transmitting multiple pulses allows the radar to increase the number of samples needed for Doppler processing, and increases the total signal-to-noise ratio (SNR). The duration of each pulse is denoted as the pulse width τ, and the duration between pulses is denoted as the pulse repetition interval. or PRI. These transmitted pulse trains will be the main source of interference between subarrays when operating with STAR capability; therefore, it is necessary to understand the properties of these pulses.

Most modern radars utilize pulse compression in order to increase their range resolution. In the absence of pulse compression, the pulse width τ determines the range resolution dR of the waveform:

$$dR = \frac{c\tau}{2}. \tag{2.8}$$

Pulse compression, however, modulates a code onto the complex envelope of the transmitted signal so that the range resolution is now given by

$$dR = \frac{c}{2\beta} \tag{2.9}$$

where β is the bandwidth of the modulation. Linear frequency modulation (LFM)

is a common modulation scheme for radar waveforms, where the frequency of the modulation is increased linearly over the duration of the pulse. The complex envelope of a LFM pulse can be given by

$$x(t) = \alpha(t)e^{j2\pi[\frac{-\beta}{2}t + j\pi\frac{\beta}{\tau}t^2]}, \qquad 0 \leq t \leq \tau \tag{2.10}$$

where the $\frac{-\beta}{2}t$ is added to allow the middle of the frequency band to occur at the radar's center frequency. The amplitude window $\alpha(t)$ denotes how the amplitude of the signal changes in time. The amplitude window used in this study was generated by the convolution of a Hann window and the magnitude of the signal. The length of the Hann window was set to a user-defined fraction of the pulse width τ. The smooth amplitude windowing of the pulse, as opposed to a rectangular amplitude windowing, was done to model smooth transitions of the waveform and reduce the amount of spectral leakage. Figure 2.5 shows both the real and imaginary components of a windowed LFM pulse.

Recall that the total signal transmitted by the array is the sum of the signals over all individual array elements

$$a_{TX}(t, \vec{K}) = \sum_{n=1}^{N} a_n(t)e^{-j\vec{K}\cdot\vec{r}_n}. \tag{2.11}$$

Ideally, the transmitted waveforms from each element will be of the same form, with possible amplitude and phase differences introduced for beamforming. However, due to hardware imperfections throughout the electronics, the transmitted signals from different channels in the array can have different frequency responses [14]. Each component in the transmit module (filters, amplifiers, phase shifters, etc.) will have a slightly different transfer function, which will produce a cascading effect of waveform distortion from the ideal. Additionally, because each element has its own

set of hardware components between the DAC stage and antenna, the distortions produced by each individual module will be unique. Because digital cancellation of the transmitted interference (discussed in Chapter 5) will require knowledge of the transmitted signals, it is important to include these imperfections in the system model. To model these waveform imperfections, each element's waveform was passed through a randomly distorted bandpass filter to model differing levels of loss through the system. The behaviour of the distortion in frequency was set to model the system used in [14]. These distortion effects on the transmitted waveforms can be most easily seen in the frequency domain. Figure 2.6 shows simulated output spectra of eight LFM pulses from a single row of array elements in the transmitting subarray. Once the waveforms were passed through the respective channel models,

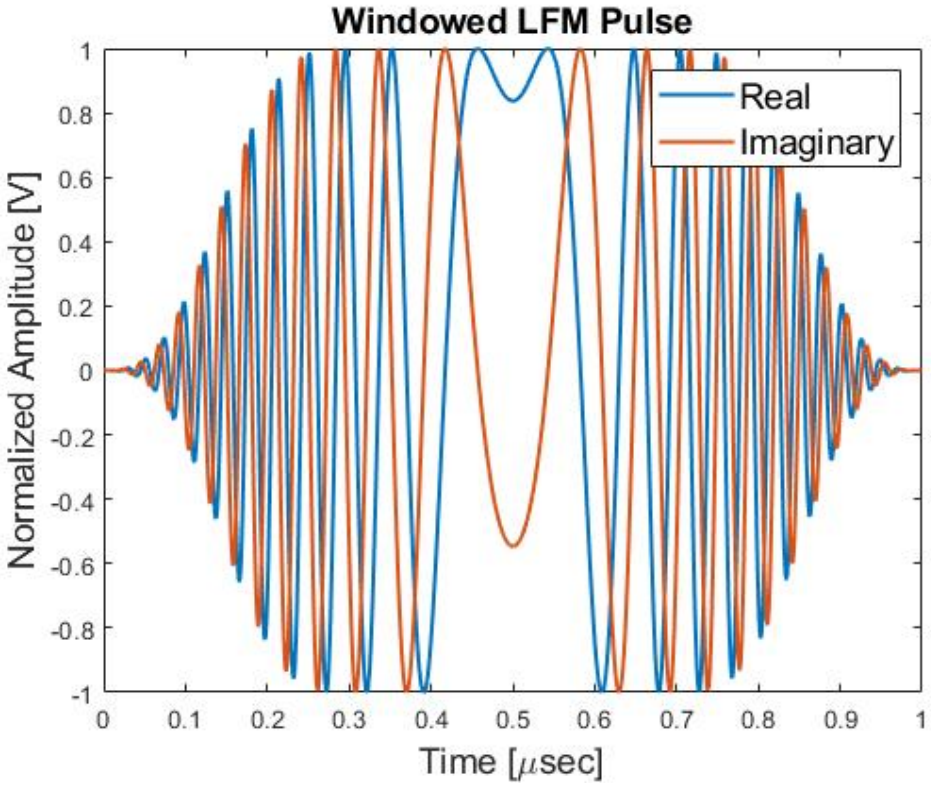

Figure 2.5: Windowed Linear-Frequency-Modulated radar pulse with a pulse with of 1 microsecond and a bandwidth of 100 MHz.

including filters, the individual waveforms contained slight mismatches that are propagated between subarrays and onto the receiving subarray antenna elements.

2.5 Transmitter and Receiver Noise

Along with waveform differences, radar noise is another practical aspect of radar systems that will affect multi-function operation. For this research, radar noise was separated into two components: transmitter noise and receiver noise.

Transmitter noise describes noise present on the transmitted radar waveforms. Transmitter noise was modeled as additive white Gaussian noise (AWGN) with a noise power independent of the transmitted waveform's power. Separating the

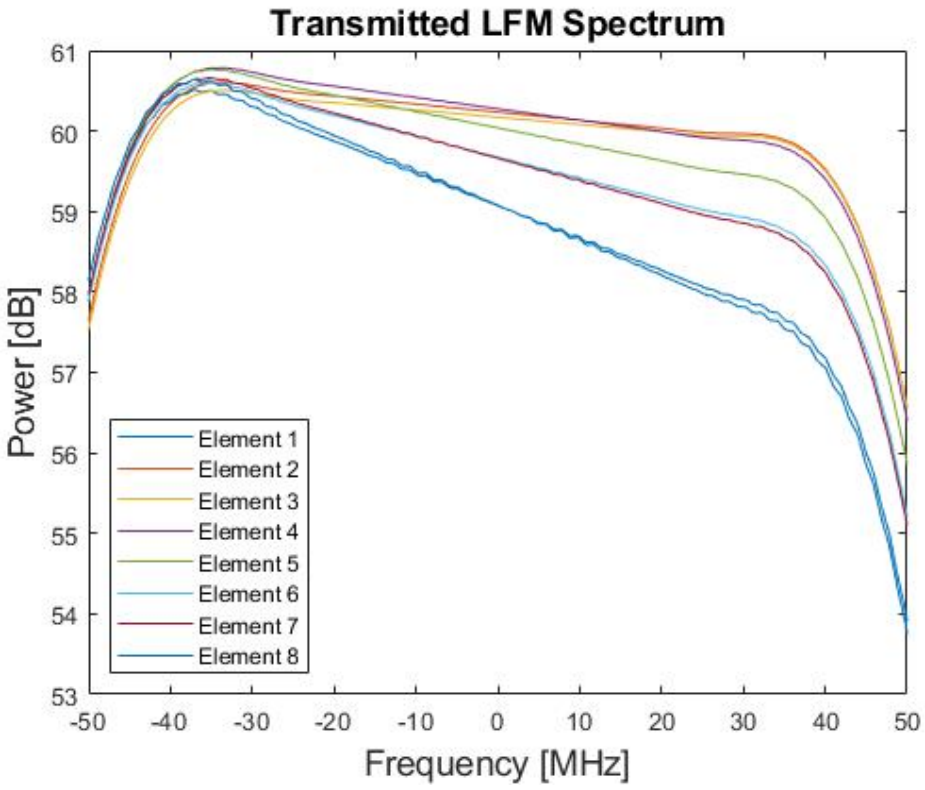

Figure 2.6: Transmitted LFM Spectrum for each element on 1 row of the transmitting subarray

noise power from the transmitted waveform power allows for the transmitted power to be increased without a corresponding increase in noise. This behaviour would correspond to the the majority of the transmitter noise being added into the signal by or after the high-power amplifier, as the noise power is not affected by changes in power amplification.

Receiver noise, defined as noise added onto the signal in the receiver chain, was also modeled as AWGN. However, the receiver average noise power was calculated according to

$$P_n = kTBF \tag{2.12}$$

where k is Boltzmann's constant, T is the operating temperature of the system in Kelvin, B is the ADC sampling rate, and F is the noise figure of each individual receiver chain [15]. The noise figure of each individual antenna element was assumed to be equal, and the receiver noise was added into the system before the LNA on each receive element to allow for differences in receiver noise amplification.

2.6 Quadrature Amplitude Modulation

In order to test the STAR capability of the array, a quadrature amplitude modulated (QAM) signal was modeled incident to the array. QAM is a modulation scheme where the signal code modulates two orthogonal sinusoids, combined in quadrature [16]. The two parallel data streams are referred to as the In-Phase signal (I) and the Quadrature-Phase signal (Q) of the IQ data. A time representation of a typical QAM signal can be seen in Figure 2.7. The number of distinct amplitudes for each orthogonal sinusoid determines the size of the signal constellation. For N distinct amplitudes, the signal constellation will have N^2 possible symbols.

The signal constellation is generated by taking samples of both the in-phase and quadrature-phase signals at each sample time T_s. Figure 2.7 shows a constellation diagram of a 16-QAM signal with $N = 4$ distinct amplitudes. Each region in Figure 2.7 signifies a specific 4-bit sequence, which can be decoded directly from the IQ signal amplitudes in each digital symbol interval. At each digital sampling period, the amplitude of the IQ data is set to match some distinct amplitude level set by the original signal. However, added noise will cause the signal amplitude to fluctuate throughout the duration of the signal. Depending on the SNR of the signal, these fluctuations could cause the signal to become unreadable. With regard to the signal constellations, the spread of the constellation points signifies the SNR of the signal: tighter constellation spreads signify higher SNR, while broader constellation spreads signify lower SNR. If the noise level is high enough to fluctuate the amplitude of the signal into another symbol's amplitude region, the decoder will output an incorrect symbol. The rate at which these errors occur is denoted as the symbol error rate, or bit-error rate (BER) when referencing the individual binary bits. Therefore the BER of the QAM signal provides a good indication of the SNR of the system. In our context, capability of the digital array depends on the array's ability to decode external signals like these QAM signals, and as such the BER can be used as a performance metric when discussing STAR performance.

Beyond just added noise, the external communications signal will also have some self-interference signal caused by mutual coupling of transmitted radar pulses to compete with, which can significantly degrade the BER of the receive subarray. The next chapter details the self-interference caused by mutual coupling.

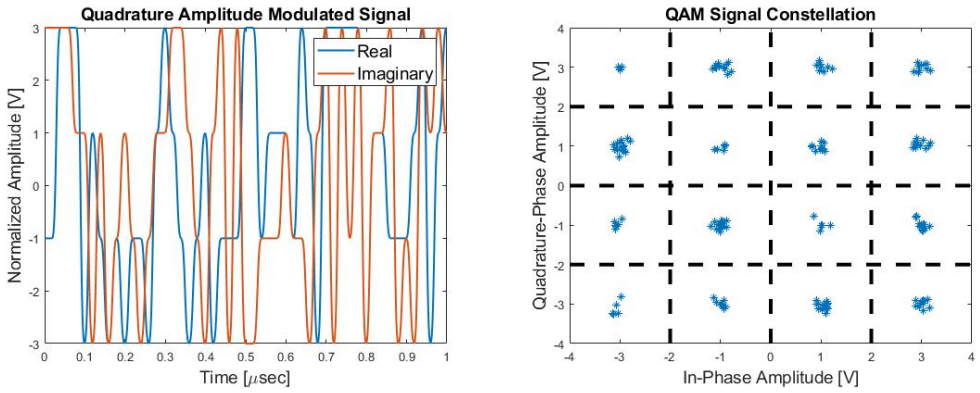

Figure 2.7: Transmitted 16-QAM signal used to measure multi-function performance in the time domain (left) and the symbol constellations (right)

Chapter 3

Mutual Coupling Analysis

Mutual coupling describes the electromagnetic interaction between elements in an array. Because of the close proximity between elements in an array (typically half-wavelength), the radiated power from a single element will have a pronounced effect on neighboring elements. When multiple elements are transmitting simultaneously, the combination of mutual coupling effects can be significant on all elements in the array. Much study has been done to develop models of mutual coupling in arrays [17, 18, 19] , as a good understanding of the mutual coupling in arrays can be beneficial in many applications [20]. One particular application of mutual coupling of interest in this thesis is how knowledge of the mutual coupling parameters can be used to describe the self-interference between elements in an array. Knowledge of the self-interference between elements generates a better understanding of how the elements in an array interact, and how the elements' behaviour can be detrimental or conducive for STAR applications. In this thesis, knowledge of the mutual coupling parameters was utilized to develop a model of the coupled signals between subarrays in a STAR aperture, and later utilized in various mitigation techniques. This chapter goes into the derivation, application, and impact of the mutual coupling parameters in an all-digital array, developed to provide an accurate simulation

of an all-digital array that can be expanded upon to test various STAR algorithms.

3.1 Theory

Recall that the total transmitted signal is the sum of all the signals generated by the transmitting elements. Let each element n have a distinct radiation pattern $f_n(\theta, \phi)$. The total radiated electric field (without mutual coupling) can be expressed as

$$E(\theta, \phi, t) = \sum_{n=1}^{N} a_n(t) f_n(\theta, \phi) e^{-jk\vec{r}\cdot\vec{r}_n} \tag{3.1}$$

where $a_n(t)$ is the complex ideal waveform present on the nth antenna element, $\vec{r}_n$ is a vector pointing to the location of the nth antenna element from the origin (center of the array), and $\vec{r}$ is a vector pointing to a region of space with direction defined by θ and ϕ. $a_n(t)$ can also be referred to as the isolated signal source on the singular antenna element from the transmission line port. However, array antennas rarely transmit from a single element at a time, and $a_n(t)$ alone is not a complete representation of the voltage present on a particular element. When multiple elements are radiating simultaneously, the voltage on the nth antenna element is the combination of the source and coupled electric fields from all transmitting elements in the array. The coupled electric fields present on a particular element are defined here as the reflections from the particular antenna's free-space boundary, and external fields produced by the other transmitting array elements. The scattering matrix of the array, denoted $\mathbf{S}$, describes the coupled fields for any pair of elements in the array. The scattering parameters are individually defined as the coupled fields on all elements when a single transmitter is transmitting. Hence, $S_{n,m}$ denotes the coupled fields *on* element n *from* element m when only element m is transmitting. The coupled fields present on each element can then be expressed in the vector $\mathbf{b}$ as

$$\mathbf{b} = \mathbf{S}\mathbf{a} \tag{3.2}$$

where $\mathbf{a}$ is now the vector of source voltages [21]. A visual representation of the coupled fields can be found in Figure 3.1. Notice that there are some reflected fields

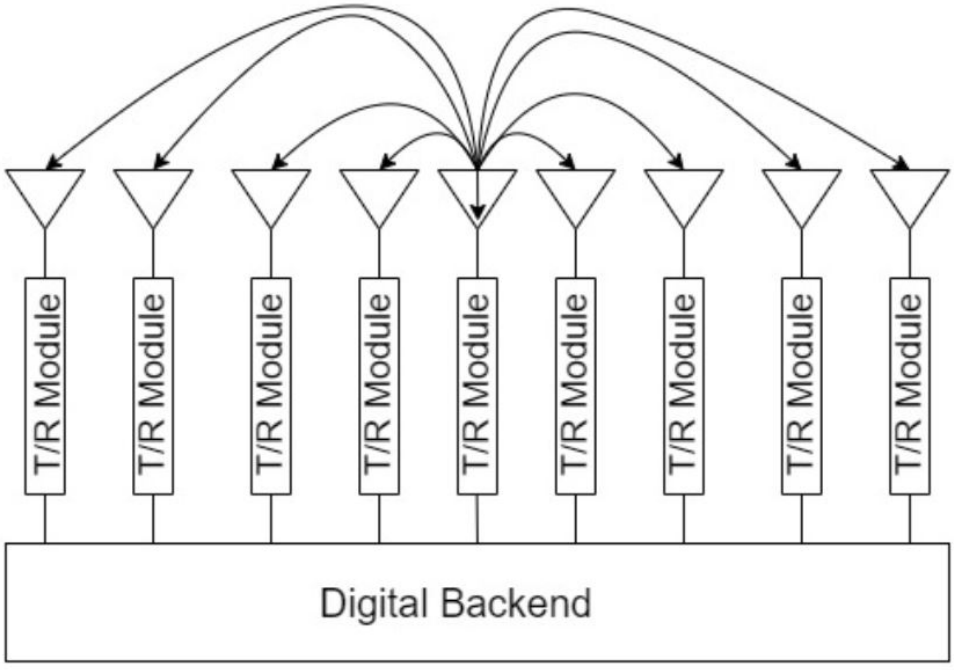

Figure 3.1: Visual representation of mutual coupling between antenna elements in an array

present on the transmitting element as well, as the antenna will not be a perfect impedance match with the environment. The voltage present at each array element is then the sum of source fields $\mathbf{a}$ and coupled fields $\mathbf{b}$

$$v_n = a_n + \sum_{m=1}^{M} \mathbf{S}_{n,m} a_m \tag{3.3}$$

The amount of energy reflected from the antenna port for a particular element is commonly denoted as the reflection coefficient. Because the goal of antennas is to

radiate energy into the atmosphere, low reflections at the antenna is desirable. When all or multiple elements of the array are transmitting simultaneously, the coupled fields incident on each element will comprise of a combination of the transmitted fields from all transmitting elements. Using this knowledge, the active reflection coefficient for a particular element m on the array can be derived as

$$\Gamma_{am} = \sum_{m=1}^{M} \mathbf{S}_{n,m} \frac{a_m}{a_n} \tag{3.4}$$

which can include the element's own reflected fields $S_{n,n}$. With uniform excitations $\mathbf{a}$ on each element in the array, the active reflection coefficient depends primarily on the physical properties of the array that determine the radiation characteristics. However, as described in Section 2.1, the complex source voltages on a particular array element $\mathbf{a}$ can be manipulated to steer collimated beams, which can produce a different excitation for each array element. Therefore, the active reflection coefficient depends not only on the physical properties of the array, but also on the beam location. As such, beam location will be an important factor to consider when analyzing the mutual coupling impact.

Now that both the source and coupled voltages have been defined, a more complete expression for the radiated electric field can be developed that includes mutual coupling effects between elements. The radiated electric field can once again be expressed as the sum of all transmitting elements, now with both source and coupled voltages present according to [22]

$$E(\theta, \phi, t) = \sum_{n=1}^{N} [a_n(t) + \sum_{m=1}^{M} \mathbf{S}_{n,m} a_m(t)] f_n(\theta, \phi) e^{-jk\vec{r}\cdot\vec{r}_n}. \tag{3.5}$$

The above expression can be simplified further by assuming all elements in the array have similar radiation patterns $f_n(\theta, \phi)$, so that an average radiation pattern

can be denoted $f_{av}(\theta, \phi)$ and brought out of the summation. This assumption is typically valid in large arrays, as the mutual coupling impact on the radiated fields is relatively uniform for elements near the center of the array. The final expression for the radiated fields is then

$$E(\theta, \phi, t) = f_{av}(\theta, \phi) \sum_{n=1}^{N} [a_n(t) + \sum_{m=1}^{M} \mathbf{S}_{n,m} a_m(t)] e^{-jk\vec{r}\cdot\vec{r}_n}. \tag{3.6}$$

Describing how the scattering parameters will impact the array signals helps to understand the benefits of including the scattering parameters in an array model, but the scattering parameters will still have to be estimated/measured to be implemented successfully in any applications.

3.2 Estimation of Scattering Parameters

Modeling and estimation of the scattering parameters of the array starts with the individual radiating element. For this research, each radiating element was modeled as a half-wave dipole antenna with a sinusoidal current distribution given by

$$I(l) = sin([l - L/2]\frac{2\pi}{\lambda}) \tag{3.7}$$

where l denotes the position on the wire, L is total length of the dipole wire, and λ is the wavelength of the signal. The impedance of the dipole Z is then given by Ohm's law according to

$$Z = \frac{V(l)}{I(l)} \tag{3.8}$$

where V is the voltage present at the dipole terminals. Because the voltage V and current I vary over the antenna, multiple different techniques for deriving the self and driving-point impedances have been well covered in the literature [23].

The technique used here is known as the induced emf method, which involves the integration of the Ponyting vector along the surface of the antenna [24]. The voltage potential on the surface of the antenna can be derived from the maximum current in cylindrical coordinates as

$$\begin{aligned} V &= \int_{-L/2}^{L/2} dV \\ &= -\frac{1}{I_m} \int_{-l/2}^{l/2} I(l = l', \rho = a) E_l(l = l', \rho = a) dl' \end{aligned} \tag{3.9}$$

where I_m is the maximum current on the element, E_l is the tangential electric field along the surface of the wire, and a is the dipole's radius. ρ is set to the dipole's radius to encapsulate the tangential electric field E_l present along the surface of the wire. The input impedance can then be expressed as

$$Z = -\frac{1}{I_m^2} \int_{-l/2}^{l/2} I(l = l', \rho = a) E_l(l = l', \rho = a) dl'. \tag{3.10}$$

Using the expression above for the input impedance and the sinusoidal current distribution, the input resistance and reactance can be approximated as [24]

$$\begin{aligned} R = \frac{\eta}{2\pi} \Big[&\gamma + ln(kl) - C_i(kl) + 0.5 sin(kl)[S_i(2kl) - 2S_i(kl)] \\ &+ 0.5 cos(kl)[\gamma + ln(kl/2) + C_i(2kl) - 2C_i(kl)] \Big] \end{aligned} \tag{3.11}$$

and

$$\begin{aligned} X = \frac{\eta}{4\pi} \Big[&2S_i(kl) + cos(kl)[2S_i(kl) - S_i(2kl)] \\ &- sin(kl)[2C_i(kl) - C_i(2kl) - C_i(\frac{2ka^2}{l})] \Big] \end{aligned} \tag{3.12}$$

where γ is the Euler-Mascheroni constant and C_i and S_i are the sine and cosine integrals

$$
\begin{aligned}
S_i(x) &= \int_0^x \frac{sin(t)}{t} dt \\
C_i(x) &= -\int_x^{\text{inf}} \frac{cos(t)}{t} dt.
\end{aligned}
\tag{3.13}
$$

These expressions for resistance and reactance are used to determine the self-impedance for each individual dipole element.

Once the self-impedance for each radiating element is determined, the next step is to determine the mutual impedance between radiating elements. For two dipoles, the mutual impedance between the two elements can be given by

$$
\begin{aligned}
Z_{21} &= \frac{V_{21}}{I_1} \\
&= -\frac{1}{I_2 I_1} \int_{-l_2/2}^{l_2/2} E_{21}(l') I_2(l') dl'
\end{aligned}
\tag{3.14}
$$

where E_{21} denotes the electric field produced by element 1 at the position of element 2. While the self-impedance was approximated assuming a sinusoidal current on a finite length dipole, the radiated electric fields used to derive the mutual impedance were assumed to be from an infinitesimal dipole, and expressed as

$$
\begin{aligned}
E_r &= \eta \frac{I_0 l cos(\theta)}{2^2} \left[1 + \frac{1}{jkr} \right] e^{-jkr} \\
E_\theta &= j\eta \frac{k I_0 l sin(\theta)}{4\pi r} \left[1 + \frac{1}{jkr} - \frac{1}{(kr)^2} \right] e^{-jkr}.
\end{aligned}
\tag{3.15}
$$

Plugging the above equations for radiated fields into (3.14) and solving the integral gives the solution for mutual impedance between two elements. Using the same procedure above for every pair of elements in the array will produce the full impedance matrix. The maximum current, dipole length, generator impedance, and current distribution were assumed to be the same for every radiating element in the array. For an N-element array, the $N \times N$ impedance matrix $\mathbf{Z}$ can be constructed that contains both the self and mutual impedance for any combination of elements.

The structure of the impedance matrix is

$$\mathbf{Z} = \begin{bmatrix} Z_{11} & Z_{12} & \cdots \\ \vdots & \ddots & \\ Z_{N1} & & Z_{NN} \end{bmatrix} \tag{3.16}$$

where Z_{nn} denotes the self impedance on the nth element and Z_{mn} denotes the mutual impedance between the mth element and the nth element.

From the mutual impedance matrix, the scattering matrix $\mathbf{S}$ of the array can be derived using [21]

$$\mathbf{S} = \frac{\mathbf{Z}/Z_0 + \mathbf{I}}{\mathbf{Z}/Z_0 - \mathbf{I}}. \tag{3.17}$$

A plot of the $\mathbf{S}$ matrix magnitude is shown in Figure 3.2 at the center frequency for a 256-element array of dipoles. One key trend to note from Figure 3.2 is the increased magnitude of $\mathbf{S}$ for elements close together (along the main diagonal) versus decreased magnitude of $\mathbf{S}$ for elements further apart (top-right and bottom-left corners). This decrease in mutual coupling magnitude versus distance will be key when examining subarray isolation for STAR functionality.

The coupling parameters $\mathbf{C}$ are another set of parameters often used for analyzing array performance. The coupling parameters can be calculated directly from the scattering parameters according to

$$\mathbf{C} = \mathbf{I} + \mathbf{S} \tag{3.18}$$

where $\mathbf{I}$ is the identity matrix of the same size as $\mathbf{S}$ [22]. Therefore, outside of the main diagonal, the scattering parameters and coupling parameters are identical. All of the parameters on the main diagonal describe the self interactions for a singular element, and are not particularly useful when examining the interaction between

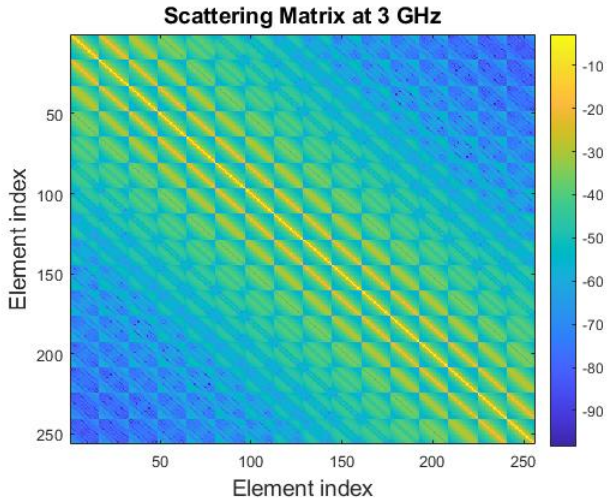

Figure 3.2: Scattering parameters of a 256 element dipole array

subarrays in a partitioned array. Because of this, the scattering parameters and the coupling parameters are often used interchangeably when solely analyzing the mutual coupling between elements in an array.

All derivations of the scattering matrix $\mathbf{S}$ up to this point have been at a single frequency. Because the waveforms transmitted by the radar will have some bandwidth, it is necessary to develop an expression for the scattering parameters for a range of frequencies that encompasses at least the signals' bandwidth. This calculation is done using the same procedure above, but changing the frequency while leaving the length of the dipoles constant. An example of the $\mathbf{S}$ parameters versus frequency that describe all the coupled fields on a singular element in a 256-element array are shown in Figure 3.3. Recall that the coupled fields present on a particular element can be split into the reflection coefficient $S_{m,m}$ and the mutual coupling between elements $S_{m,n}$.

The reflection coefficient of the element has a markedly different response compared to the inter-element coupling, as low reflections at the center frequency are desired. It is also important to notice that the magnitude of the mutual coupling

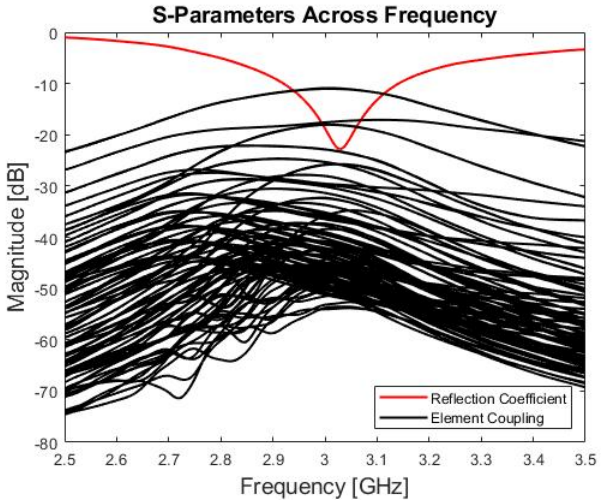

Figure 3.3: Scattering parameters for a singular element in a 256 element dipole array

varies considerably for different pairs of elements. Elements with close proximity to one another typically experience higher magnitudes of mutual coupling, as the magnitude of the mutual coupling declines as the distance between elements is increased. While the majority of the mutual coupling magnitude is relatively weak, the summation of all of the coupled signals on a singular element will be a significant hindrance toward STAR operation.

While the mutual coupling parameters modeled in this section were modeled using dipole elements, the same procedure could be implemented using any other type of antenna element. The important parameter of the antenna element that would be needed to develop a good model of the mutual coupling parameters would be the expressions of the radiated electric fields generated by the antenna elements. Depending on the antenna element, an accurate solution for the radiated electric fields may or may not be easily derived. In practice, the scattering parameters for an array can be measured directly, albeit with added uncertainty due to noise.

3.3 Application

Once a good model of the scattering matrix has been developed, the next step is applying the scattering parameters to the transmitted waveforms. Recall that the scattering parameters were estimated over a wide range of frequencies in order to encompass frequencies that include at least the bandwidth of the waveform. Because the coupling parameters vary in frequency, the application of the scattering matrix can be modeled as a multiplication of the transmitted waveform spectra and the scattering parameters $\mathbf{S}$ in the frequency domain. For a segmented STAR array, the primary impact of mutual coupling is found between transmitting subarrays and non-transmitting subarrays. Signals from the transmitting subarray elements will pass through the coupling channels modeled using the $\mathbf{S}$ parameters, and be reflected onto the non-transmitting subarray elements. If the non-transmitting subarray elements are being used to receive some external signal, the coupled signals can be detrimental to the receive subarray performance. These coupled signals from the transmitted subarray are referred to as leakage signals, describing how the power from the transmitting subarray "leaks" onto the receive subarray elements. The received vector of leakage signals $\mathbf{b}$ can be described in the frequency domain as

$$\mathbf{b}(F) = (\mathbf{S}(F) + \Delta\mathbf{S}(F))(\mathbf{a}(F) + \Delta\mathbf{a}(F) + \sigma_{TX}) \odot \epsilon + \sigma_{RX} \tag{3.19}$$

where $\mathbf{a}(\mathbf{F})$ is the vector of transmitted spectra with uncertainty $\Delta\mathbf{a}(F)$, $\mathbf{S}(F)$ is the matrix of mutual coupling parameters with uncertainty $\Delta\mathbf{S}(F)$, receiver amplitude and phase errors ϵ, and transmitter and receiver noise σ_{TX} and σ_{RX}, respectively. Uncertainties in the waveforms can come from hardware imperfections from different element modules or distortions from high-power amplifiers. Scattering matrix

uncertainties come from the inability to perfectly measure/estimate scattering parameters in practice.

Because all the parameters of the array are modeled at discrete frequencies, the equation above can be implemented using a matrix multiplication of the transmitted signal vector $\mathbf{A}(F)$ and the mutual coupling matrix $\mathbf{S}(F)$ for every discrete frequency value. In other words, if there are N discrete frequency values in the model of the waveform, there will be N matrix multiplications to generate the leakage signals over frequency $\mathbf{b}(F)$. Once the leakage signals are derived in the frequency domain, an inverse Fourier transform is used to obtain the distorted leakage signals in the time domain. Figure 3.4 shows how the scattering parameters can be applied in the frequency domain to generate the leakage signal for one pair of elements. The transmitted signal spectrum in Figure 3.4 was normalized to better show how the distorted leakage signal will be derived directly from the wide-band scattering parameters. While the magnitude of the individual leakage signal is quite small, the total leakage signal on a single receive subarray element will be the combination of all transmitted pulses through each respective coupling channel pair. The summation of these leakage signals can therefore have a major impact on the receive subarray performance.

3.4 Array Impact

Mutual coupling effects can have a dramatic impact on the performance of the array. Many studies have investigated the impact mutual coupling has on the array radiation patterns [17]. While mutual coupling effects on radiation patterns will be an important factor to consider when designing phased arrays, for an array utilizing STAR with multiple subarrays, the mutual coupling impact will have the most

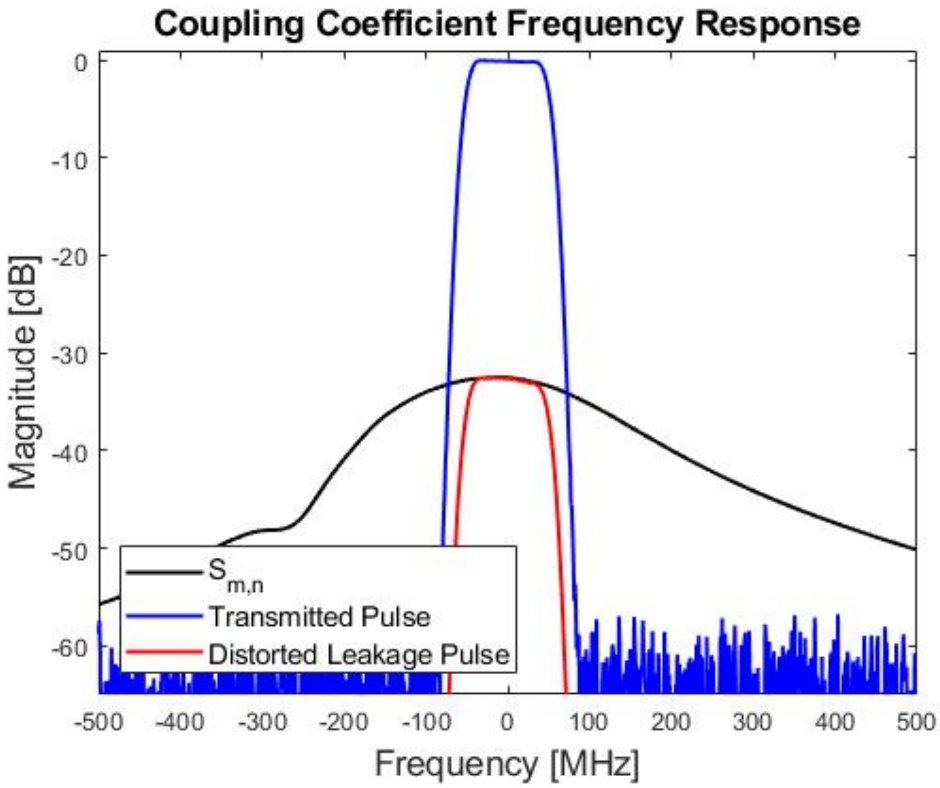

Figure 3.4: Application of coupling coefficients in the frequency domain. Total leakage signal is the combination of distorted pulses from all transmitting elements.

pronounced impact directly on the receive subarray. This impact can be best exemplified by the high-power leakage signals incident on the receive subarray. To observe the leakage power between adjacent subarrays, a simulated 16×16 array was split vertically into two equally sized subarrays, with one subarray transmitting LFM pulses and the other subarray receiving external signals. The leakage signals incident on the receive subarray elements were then calculated according to the procedure outlined in Section 3.3. The average leakage power for each receive subarray element can be found in Figure 3.5, with the specified saturation limit of the ADC on each element. As expected, the highest power leakage signals are found on the columns most adjacent to the transmitting subarray. However, as the physical distance between subarrays is increased, the leakage power is decreased. This de-

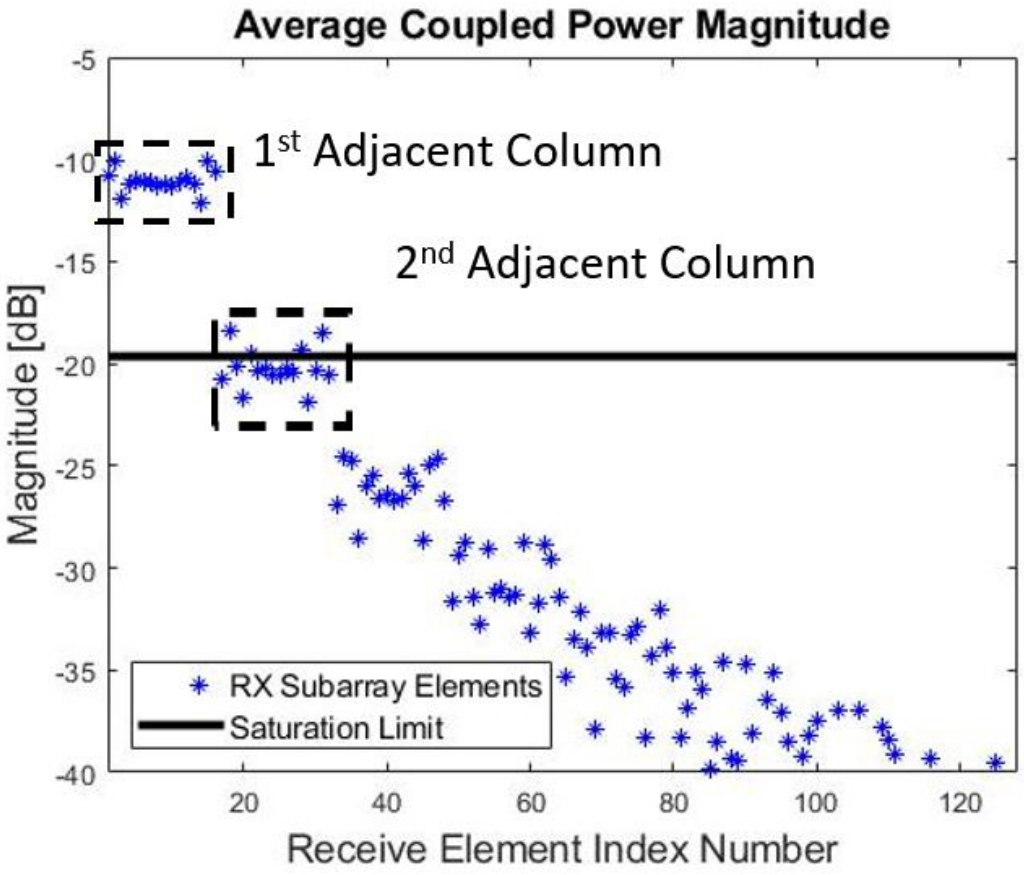

Figure 3.5: Average leakage power for each element in the receive subarray. Adjacent columns to the transmitter are marked for clarity.

crease in leakage power is due to the attenuation of the transmitted signals as they travel through the medium around the array.

The saturation of the receive subarray elements will also be an important factor to consider when examining STAR capability. The level of the saturation limit depends on a couple factors: the minimum detectable voltage and the number of ADC bits available. These two values define the dynamic range of the receiving element, which encompasses values from the least significant bit (LSB) to 2^N times the LSB, where N is the number of binary bits. While the dynamic range is set by the number of ADC bits available, the saturation limit of the ADC can be user-defined.

Higher saturation limits will reduce the sensitivity of the ADC (set by the LSB), while allowing accurate conversion of higher power signals. Lower saturation limits, conversely, will increase the sensitivity of ADC, while being more susceptible to saturation. The saturation limit of the ADCs used for Figure 3.5 was kept constant for each element in the array, however in practice it may be possible to configure the limits separately. Although the dynamic range can be adjusted, having multiple saturated elements due to adjacent transmitters provides a good baseline to examine STAR capabilities.

While transmitted signal leakage will be the primary source of interference to the receiving subarray in STAR operation, transmitter noise will also have an impact on the receive subarray elements due to mutual coupling. Transmitter noise will go through the same coupling paths as the transmitted signals, and will be reflected onto the receivers. Typically, transmitter noise levels from target reflections are low enough that the transmitter noise is below the receiver noise for reflected radar signals; However, when transmitting high-power signals, the coupled noise transmitted between subarrays can be stronger than the receiver noise. This coupled noise level will be dwarfed by the leakage signal power, but implementation of digital cancellation techniques in Chapter 5 can leave a residue noise level that will be at least as large as the coupled noise level in some scenarios. Therefore, the transmitter noise level can be a limiting factor on the receive subarray dynamic range when transmitting at high-power levels.

Saturated elements on the receive subarray also pose a significant problem on the receive subarray performance. If a particular element is saturated, many of the desired signal properties found in the complex envelope of the waveform will be distorted or irrecoverable, making many signal processing techniques obsolete. Digital cancellation of the leakage signals in particular becomes challenging when

analyzing saturated signals. Because of these challenges, any elements that were saturated were deemed unusable and discarded for this study. Discarding saturated elements causes a dramatic decrease in receive gain and limits the data available for angle of arrival estimates. It is easy to see then how reducing the leakage signal power below saturation will have a profound impact on the STAR capability of the array. Reducing the leakage signal power is the focus of the next chapter, which details how adaptive beamforming techniques can be utilized to reduce leakage power.

Chapter 4

Adaptive Beamforming

Traditional beamforming in an array antenna is used to steer the constant phase front of propagating signals in a particular direction. Beamforming is accomplished by adjusting the amplitude and phase of the signal on each individual element in the array with a vector of beamforming weights, so that phases of the transmitted signal are aligned in some particular direction in space. Adaptive beamforming uses these beamforming weights to optimize the array pattern according to some desired response. Common examples include maximizing the gain in a particular direction, or creating nulls in the array pattern to minimize jamming signals from a particular direction while continually scanning the beam [25]. In most scenarios, radar signals are transmitted with beamformers designed to maximize the transmitted power in a particular direction as maximizing the transmitted power allows radars to receive reflections from targets at extended ranges. When an array is operating with multiple subarrays for STAR capability, transmitting with high power on one subarray for radar operation leads to high power leakage signals present on adjacent subarrays. These leakage signals can dominate any external signals of interest, and can saturate receive subarray elements that are in close proximity to the transmitting subarray. To combat these high power leakage signals, an adaptive transmit beamformer can be designed to limit the leakage power incident onto another subarray.

Conversely, an adaptive receive beamformer can be designed to weight the receive subarray elements to maximize the signal-to-interference-plus-noise ratio (SINR), where the interference is defined as the mutually coupled signals from the transmitting subarray. This chapter is an examination of how adaptive beamforming can be used to minimize leakage power between subarrays and maximize SINR in a STAR array.

4.1 Theory

Before investigating how adaptive beamforming weights can be used to minimize leakage power, it is first necessary to understand the implementation of classical beamformers. Beamformers are designed to tune the collimated beam of the array to some desired response. These responses can be created for a length N array by applying the complex spatial array weights,

$$\mathbf{w}[n] = W_n e^{j\psi_n} \tag{4.1}$$

where W_n is the amplitude of the nth array element and ψ_n is the phase of the nth array element's weight. Phase changes on the beamforming weights are typically used to steer the beam, while amplitude changes are used to control the shape of the array factor. Using the signal model derived in Chapter 2, the non-adaptive beamforming weights for a transmitting radar can be more specifically defined as

$$\mathbf{w}_{TX}[n] = W_n e^{j\vec{\mathbf{K}}_{TX}\cdot\vec{\mathbf{r}}_n} \tag{4.2}$$

where $\vec{\mathbf{K}}_{TX}$ defines the desired steering location and $\vec{\mathbf{r}}_n$ is the vector pointing to the location of the nth element in the array. The transmitted signal therefore is

maximized in the direction defined by $\vec{\mathbf{K}}_{TX}$.

When utilized in a STAR array that is partitioned into subarrays, adaptive beamforming can be used to provide improved isolation between subarrays. Specifically, the scattering parameters of the array $\mathbf{S}$ can be used to describe the direct-path interference between subarrays, which can then be mitigated using adaptive beamforming techniques [26].

4.2 Adaptive Transmit Beamformer

An adaptive transmit beamformer can be designed to minimize the leakage power from adjacent subarrays. Before transmission, each of the N signals on transmitting elements will pass through a complex beamformer, $\mathbf{w}_{TX}$. The Nx1 vector of transmitted signals can then be expressed as

$$\mathbf{y}_{TX}(t) = \mathbf{w}_{TX} \odot \mathbf{a}(t) + \sigma_{TX}(t), \tag{4.3}$$

where $\mathbf{a}(t)$ is the vector of transmitted signals in the time domain and $\sigma_{TX}(t)$ is the additive white gaussian noise present on each transmitting element. Each transmitted signal from element n will go through a unique coupling path $\mathbf{s_{m,n}}(t)$ before being reflected onto element m. The coupling path $\mathbf{s_{m,n}}(t)$ is modeled as a linear time-invariant (LTI) system defined by the scattering parameters calculated across frequency in Chapter 3, so that it can be easily applied in both the time and frequency domains. The Mx1 vector of received leakage signals is given by

$$\mathbf{y}_{int}(t) = \sum_{n=1}^{N} \mathbf{s}_{:,n}(t) \circledast y_{tx}[n,t). \tag{4.4}$$

where $y_{tx}[n,t)$ denotes the time-domain signal transmitted from the nth element at time t and $\circledast$ denotes convolution. The bracket in $y_{tx}[n,t)$ is used to denote the

discrete and finite number of array elements N. Because the coupling paths are modeled as LTI systems, the convolution above can be applied in the frequency domain as a multiplication of the scattering parameters across frequency and the transmitted signal spectra. The leakage signals in an array environment with N transmit elements and M receive elements can then be expressed in terms of the vector of transmitted signal spectrum $\mathbf{Y}_{TX}(F)$ and the scattering matrix versus frequency $\mathbf{S}(F)$ as

$$\mathbf{Y}_{int}(F) = \mathbf{S}(F)\mathbf{Y}_{tx}(F). \tag{4.5}$$

Although the coupling parameters vary across frequency, beamforming weights are typically derived using the center frequency of the waveform, unless true-time-delay phase shifters are applied. Therefore, for the sake of calculating the adaptive beamforming weights, the equation above can be simplified further by assuming the coupling parameters are relatively constant throughout the bandwidth of the transmitted signal, so that the multiplication in the frequency domain can be approximated as a single matrix multiplication of the coupling parameters and the transmitted signal spectrum at the center frequency of the waveform f_0. While analyzing the coupling parameters only at the center frequency will not provide a complete description of the leakage signals, the behaviour at the center frequency does provide a good indication of the total leakage power. Using this assumption, the total leakage power incident on the M receive subarray elements can be approximated as

$$P_{int} = E[\mathbf{Y}_{int}^H \mathbf{Y}_{int}] = \mathbf{Y}_{TX}^H \mathbf{S}^H \mathbf{S} \mathbf{Y}_{TX} \tag{4.6}$$

where $\mathbf{S} = \mathbf{S}(F = f_0)$, $\mathbf{Y}_{int} = \mathbf{Y}_{int}(F = f_0)$, and $\mathbf{Y}_{TX} = \mathbf{Y}_{TX}(F = f_0)$.

Assuming the transmitted signals are the same on each channel before passing

through the transmit beamformer $\mathbf{w_{TX}}$, the leakage power can be simplified further into

$$P_{int} = P_{TX}[\mathbf{w}_{TX}^H \mathbf{S}^H \mathbf{S} \mathbf{w}_{TX}] + \sigma_{tx}^2[\mathbf{w}_{TX}^H \mathbf{S}^H \mathbf{S} \mathbf{w}_{TX}]. \tag{4.7}$$

Clearly, the transmit beamforming weights $\mathbf{w}_{TX}$ will have a significant impact on the total leakage power reflected onto the receive subarray. Therefore the weights should ideally be selected in a way that minimizes the leakage power, while maintaining a peak gain of the transmitted signal in a desired direction [27]. Let $\mathbf{C}$ be the non-adaptive beamforming weights required to steer the beam in a particular direction. The minimization problem can be denoted as

$$\begin{aligned} \underset{\mathbf{w}_{TX}}{\text{minimize}} \quad & \mathbf{w}_{TX}^H \mathbf{S}^H \mathbf{S} \mathbf{w}_{TX} \\ \text{subject to} \quad & \mathbf{C}^H \mathbf{w}_{TX} = 1. \end{aligned} \tag{4.8}$$

The optimization problem above can be solved using a stochastic gradient descent method [28], where each new set of beamforming weights $\mathbf{w}_{TX}$ is determined by

$$\mathbf{w_{TX}}[\mathbf{n+1}] = \mathbf{w_{TX}}[\mathbf{n}] - \mu[\mathbf{R}\mathbf{w_{TX}}[\mathbf{n}] + \mathbf{R^H}\mathbf{w_{TX}}[\mathbf{n}] + \lambda \mathbf{C}]. \tag{4.9}$$

$\mathbf{R}$ is the correlation matrix of the mutual coupling channels, $\mathbf{R} = \mathbf{S^H S}$, μ is the step-size parameter, and λ is the Lagrange multiplier set to

$$\lambda = \frac{-1}{\mathbf{C^H}(\mathbf{R} + \mathbf{R^H})^{-\mathbf{1}}\mathbf{C}}, \tag{4.10}$$

which enforces the desired gain in the steering direction [29]. The iterative process above can be said to converge when the leakage power P_{int} varies less than ϵ between successive iterations. The variation in leakage power P_{int} for each iteration of beamforming weights calculated in (4.9) is shown in Figure 4.1, with ϵ set to

0.1%. Looking at the curve in Figure 4.1, the leakage power converges after approximately 2000 trials and reduces the leakage power by almost 30 dBW. Once the adaptive weights have been determined, it is important to examine how the new beamforming weights will affect the transmitted radiation patterns.

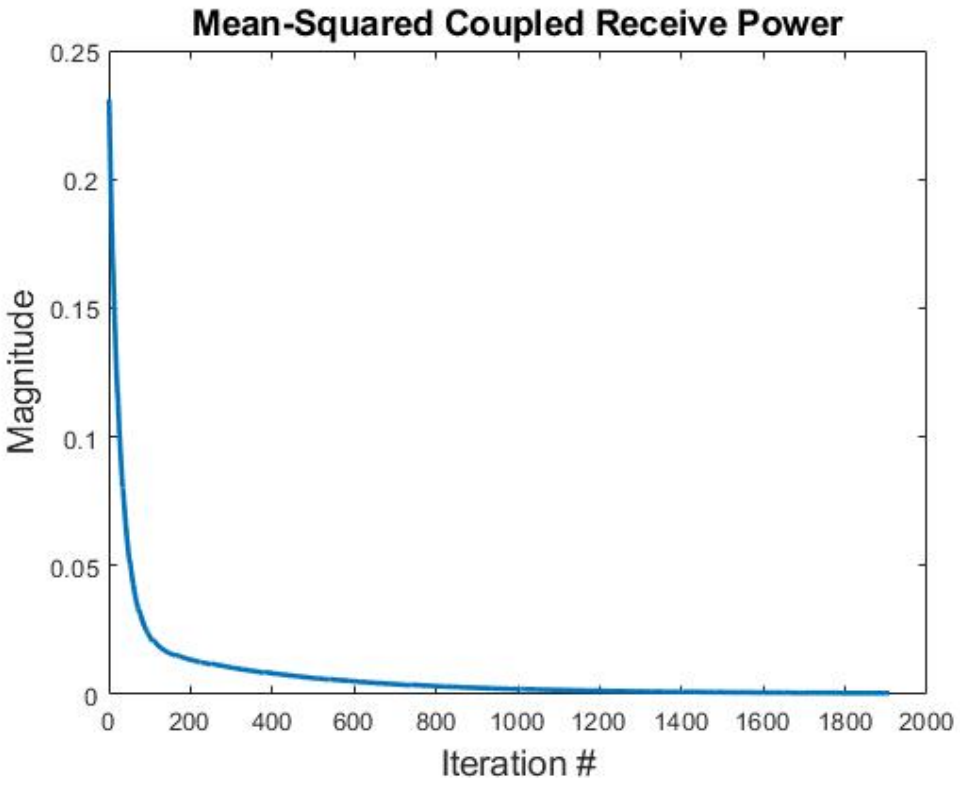

Figure 4.1: Mean-squared leakage power as a function of adaptive iterations

4.3 Impact on Transmit Subarray

The use of any adaptive weighting scheme beyond uniform weighting will have some impact on the transmit subarray performance as it relates to the transmitted beam shape. Some performance degradation of the transmitted beam can be tolerated provided benefits in the receive subarray SNR, so it is worthwhile to investigate the transmit subarray properties of each weighting scheme. Some important aspects

of the transmit subarray beam to look at include the beamwidth, peak gain, and sidelobe level, as they will all be directly impacted by the change in beamforming weights. The adaptive weights calculated above were compared to both a uniform beamforming scheme and a beamforming scheme with one column of guard elements (zero transmission) between the transmit and receive subarrays. The guard elements would be taken from the transmitting subarray. The guard elements would not be utilized in either subarray, and are produced only to increase subarray isolation. The one-column guard scheme would be a simple and straightforward way to potentially increase isolation between the transmit and receive subarrays, and could be a good alternative to the adaptive beamforming scheme for comparison.

To compare different beamforming schemes, a simulated 16×16 array of elements was split into two equally sized subarrays, positioned side-by-side along the azimuth plane of the array. One of the subarrays was transmitting signals while the other was focused on receiving external signals. Table 4.1 below compares some of the array parameters for different beamforming weights.

As expected, the uniform weights produce the highest transmit gain and aperture efficiency, while also providing the highest levels of leakage power. The aperture efficiency of the subarray was calculated according to

$$\epsilon_w = \frac{|\sum w[n]|^2}{N \sum |w[n]^2|}. \tag{4.11}$$

	Uniform Weights	Adaptive Weights	1-Column Guard
Transmit Gain	42.1 dB	39.8 dB	40.9 dB
Aperture Efficiency	1.00	.909	.875
Leakage Power	-6.4 dB	-35.4 dB	-12 dB
θ_{3dB} (Elevation)	6.35°	6.4°	6.35°
θ_{3dB} (Azimuth)	12.7°	14°	14.6°

Table 4.1: Comparison of different transmit beamforming schemes

In 4.11, $w[n]$ corresponds to the beamforming weight applied at each element n. The leakage power in Table 4.1 only includes contributions from the center frequency (P_{int} as defined above), but gives a good approximation of the total leakage power improvement given by the adaptive beamformer. Compared to the 1-column guard beamformer, the adaptive beamformer does produce a larger reduction in gain, while maintaining a slightly narrower beamwidth in the azimuth plane. The key difference between the adaptive weights and the 1-column guard weights is seen in the leakage power; The 1-column guard weights reduce the leakage power almost 6 dBW from the uniform case, while the adaptive weights provide a leakage power reduction of almost 30 dBW at the center frequency. This leakage power reduction will have a major impact on the receive subarray performance.

Figure 4.2 gives a comparison of the traditional uniform weighted beamformer pattern to the calculated adaptive beamformer pattern, calculated both at broadside and steered off-axis to show the capability of the adaptive beamformer to still steer the beam. It is evident from Figure 4.2 that the majority of the pattern distortion occurs along the principle plane of the array partition, which is along the azimuth plane in this scenario. There is a small reduction of gain in the elevation plane, but otherwise the patterns remain consistent along the elevation plane. The half-power beamdwidths of each plane also follow this trend, as shown in Table 4.1.

This section has outlined the impact of adaptive transmit beamforming on the transmitted patterns. While the adaptive beamforming scheme shown above does produce a reduction in gain for a far-field radar target, the reduction in coupled leakage power on the receiving subarray can provide substantial benefits toward the STAR operation of the array.

4.4 Impact on Receive Subarray

It is important to ensure that any beamforming scheme used on transmit has the desired leakage reduction on the receive subarray. As shown in Section 4.3, adaptive transmit beamforming schemes were designed to reduce the coupled leakage power on the receiving subarray by reducing the peak gain achievable by the transmitting subarray. If the reduction in leakage power is minimal, the peak gain reduction on the transmitting subarray might be unwarranted. As discussed in Chapter 3, a big obstacle to achieving STAR is leakage power significant enough to saturate elements on the receive subarray. Once an element reaches the saturation point, the data acquired from that element serves almost no use, and it is impossible to utilize any digital cancellation techniques to increase the SINR. Therefore the key metric of performance for any transmit beamforming scheme, as it relates to STAR capability is the impact on the number of saturated elements on the receive subarray. To test how different beamforming schemes can affect the number of saturated elements, the same vertically split array configuration (two 16×8 subarrays) from

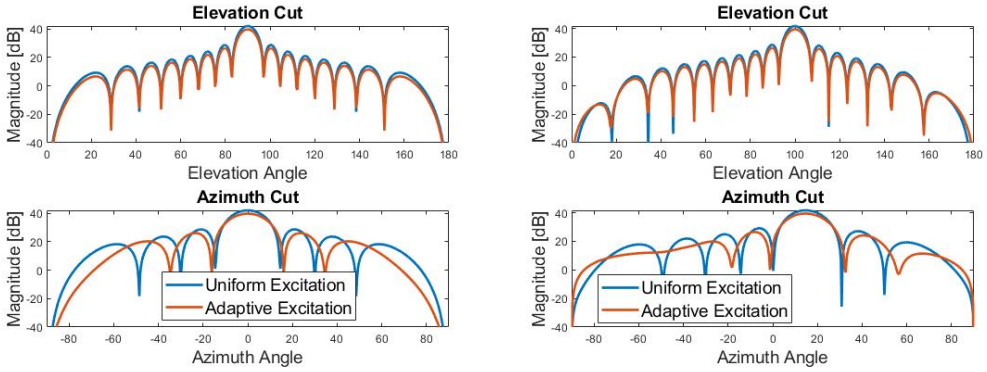

Figure 4.2: Array radiation patterns utilizing the adaptive beamforming weights normal to the array (left) and steered off-axis (right). The array was split into side-by-side horizontal subarrays, corresponding to the azimuth principle plane.

Section 4.3 was utilized to record the number of saturated receive subarray elements for different transmit power levels (per element). The 16×8 transmitting subarray was transmitting 100 MHz LFM signals, centered at the resonant frequency of the estimated scattering parameters. The number of saturated elements on the receiver for each beamforming scheme and transmit power level can be found in Figure 4.3. It is important to note that while the number of saturated elements will depend heavily on the ADC stage (number of bits, lowest bit, etc.), the same general trends of saturation will remain constant. The adaptive beamforming scheme has the best performance in terms of saturated elements, as the transmitter was able to transmit up to 400 W before saturating any elements. This performance shows that while the adaptive beamformer has the largest peak gain reduction on the transmitted beam, it also provides the highest level of leakage suppression between subarrays. The 1-column guard beamforming scheme also performed better than uniform at lower transmit powers, but followed an interesting trend as the transmitter power level was increased; The number of saturated elements using the 1-column guard scheme increased at a much faster rate than either the uniform weighting or the adaptive weighting. This behaviour can best be shown by looking at the average leakage power levels for each element in the receive subarray individually, as shown in Figure 4.4. Even though the 1-column guard beamforming scheme does produce the desired reduction in leakage power for the elements closest to the transmitting subarray (lower element numbers), the average leakage power does not decrease across the array nearly as fast as with the uniform weighting scheme. This behaviour can be attributed to the constructive versus destructive interference seen at each receive subarray element from the sum of *all* transmitting elements, described by the scattering parameters. Even though the number of transmitting elements is decreased by the addition of the 1-column guard, at regions further away from the transmit-

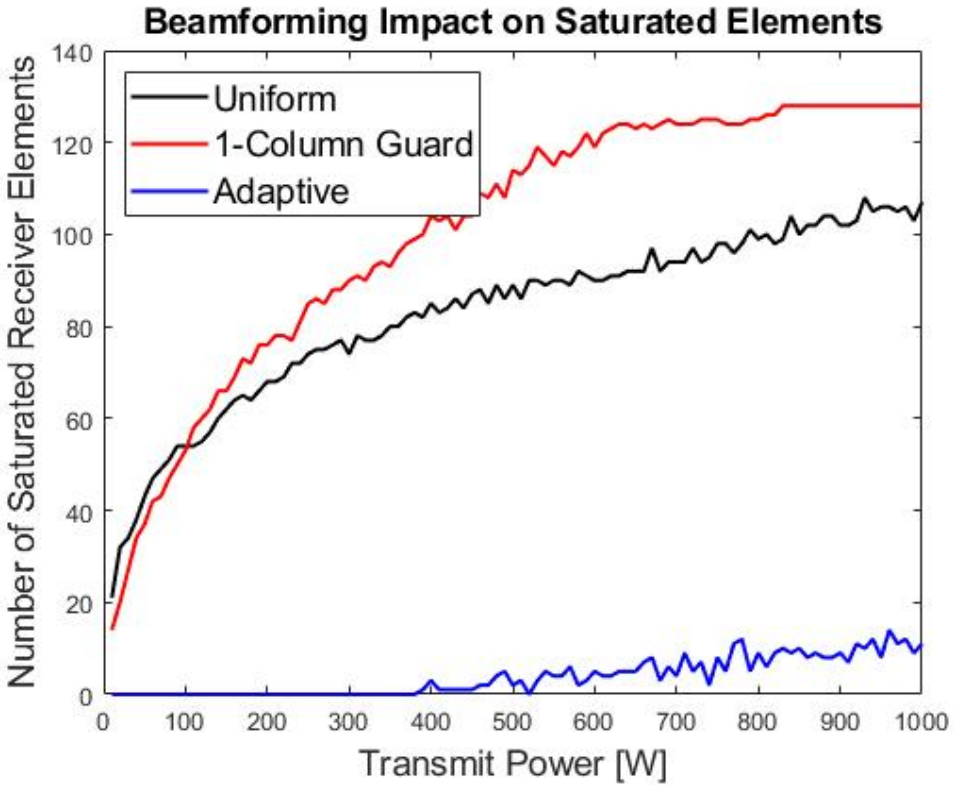

Figure 4.3: Comparison of the number of saturated elements for different transmit beamforming schemes

ting subarray, the constructive interference of the remaining transmitting elements exceeds the levels produced by the uniformly weighted transmitting scheme. It is worth noting here that the constructive versus destructive behaviour of the leakage signals is heavily dependent on the scattering parameters, and that this result for a 1-column guard between subarrays may not always be realistic. The key take-away is the dependency of the leakage signals on the scattering parameters, which can be taken advantage of by using the adaptive beamforming weights and should be considered when implementing any beamforming scheme. The adaptive beamforming scheme, because it was calculated directly from the scattering parameters, reduces the leakage power seen at every element in the receiver. Figure 4.5 gives a visual representation of the leakage power produced by each beamforming scheme

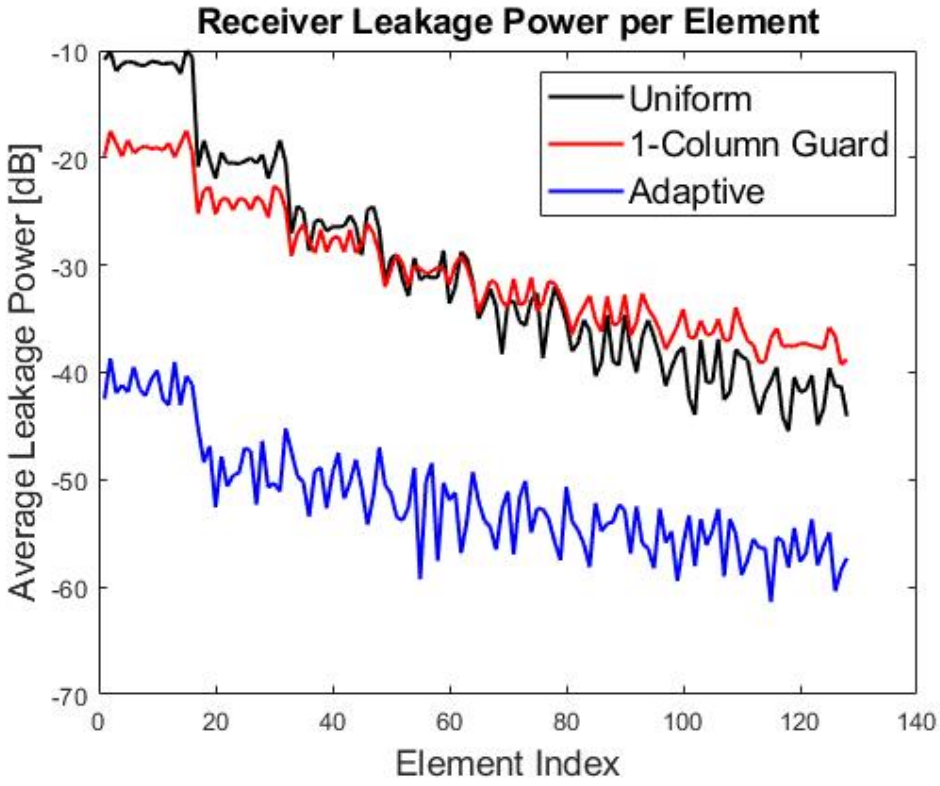

Figure 4.4: Comparison of average leakage power per receiver element under different beamforming schemes

by showing the transmitter power levels and leakage power levels for every element in the array. In this orientation, the array was transmitting from the left eight columns and receiving from the right eight columns. The plotted values are either the transmitted power or leakage power levels, depending on the element's position in the array.

Looking at Figure 4.5, the impact of the adaptive transmit beamformer is apparent. The leakage power levels produced by the adaptive beamforming scheme are significantly lower throughout the receive subarray when compared to either of the other two beamforming schemes. The high levels of constructive interference on receive subarray elements from the one-column guard beamforming scheme is easily seen as well, as the leakage power levels in the furthest elements are notice-

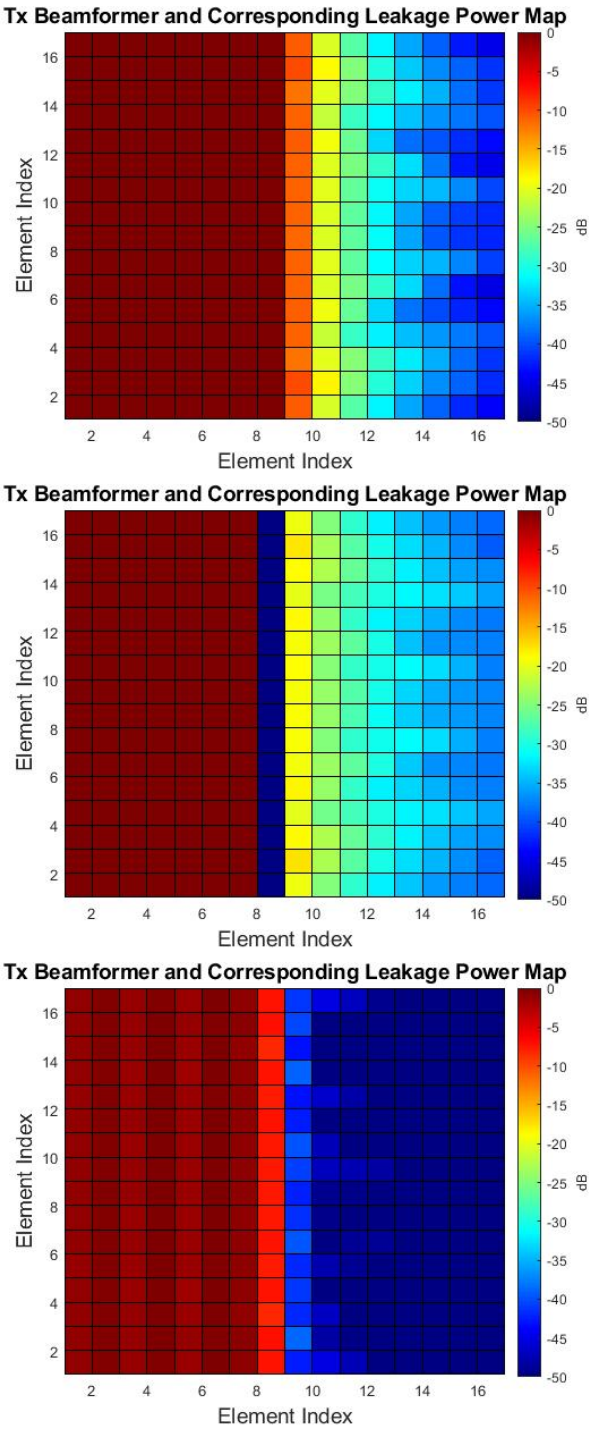

Figure 4.5: Power maps of 3 different transmit beamforming schemes: uniformly weighted (top), 1-column guard (middle), and adaptive (bottom). The array was transmitting on the left half of the array, with incident leakage on the right half.

ably higher than for the uniform beamforming scheme. The uniform beamforming scheme would present the baseline performance of the array, without any attempt to increase isolation between subarrays. Clearly, taking advantage of the destructive interference of the signals by use of adaptive weighting is highly beneficial. The destructive interference levels will be highly influenced by the scattering parameters, and as such the scattering parameters should be considered when designing any beamforming scheme to reduce the leakage power levels to ensure the desired behavior is obtained. While the adaptive beamforming weights produce the lowest levels of leakage power, their dependence on the coupling parameters of the array could result in performance degradation as the uncertainties in the coupling parameters are increased. Therefore, it is desirable to examine the sensitivity of the adaptive transmit beamformer performance to coupling parameter uncertainty.

4.5 Sensitivity to Mutual Coupling Estimation

Because the adaptive transmit beamforming weights are calculated directly from the coupling parameters, the accuracy of the coupling parameters will have a significant impact on the performance of the transmit beamformer. To test the impact of coupling parameter uncertainties, normally distributed random errors were added into the coupling parameters (both real and imaginary parts) used to calculate the adaptive weights. The standard deviation of the random errors was set to some percentage of the value of each coefficient. Even though the calculation of the adaptive weights only uses the scattering parameters at the center frequency of the transmitted waveforms, uncertainty was added to all coefficients of the coupling matrix versus frequency in the system to determine the impact of the uncertainties. Figure 4.6 shows the ability of the adaptive transmit beamformer to reduce the av-

erage leakage power for varying levels of scattering matrix uncertainties and with the transmitting subarray transmitting -10 dBW per element.

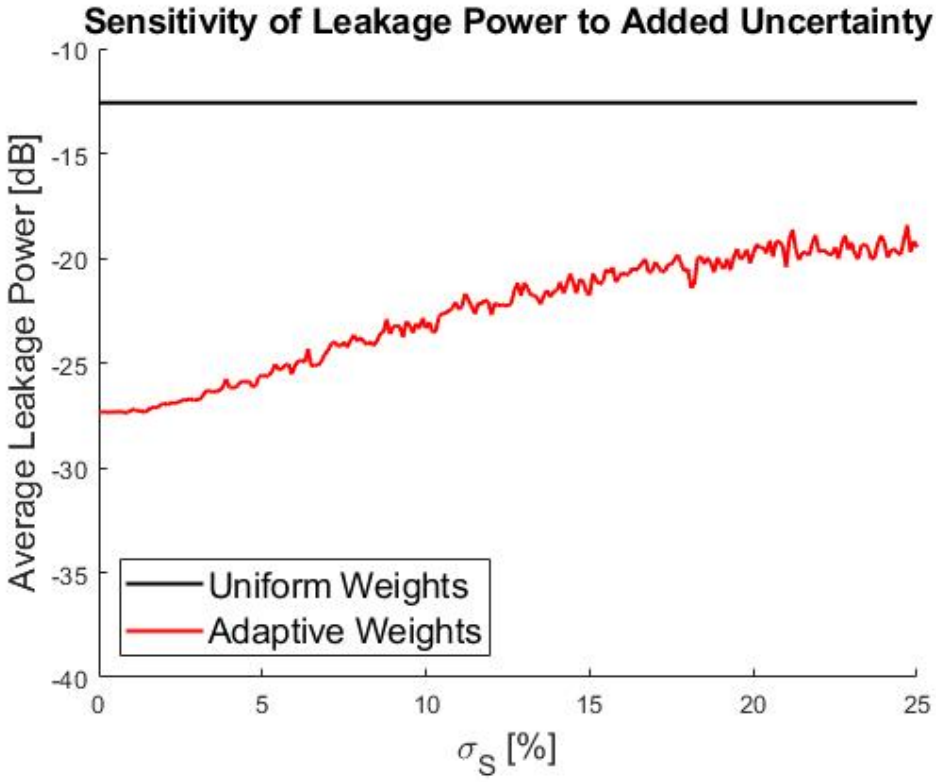

Figure 4.6: Average leakage power as a function of S-matrix uncertainties utilizing both uniform and adaptive beamforming weights

Differences in the transmitted waveforms and transmitter/receiver noise produce a non-smooth curve of leakage power values. Even though each of the values shown in Figure 4.6 was averaged over 20 trials, there is still some variant behaviour seen in the curve. However, the trend of performance is still clear: as uncertainties in $\mathbf{S}$ are increased, the ability of the adaptive beamformer to reduce the leakage power is degraded. Still, there is a substantial benefit of the adaptive weights compared to the beamforming weights even with the added uncertainty in $\mathbf{S}$. This result is promising, as it will be impossible to get a perfect measurement of $\mathbf{S}$ in practice, and any beamforming scheme will need to be robust to uncertainty.

4.6 Transmitted Beam Position Impact

Because the beamforming weights $\mathbf{w}_{TX}$ are complex values depending on the desired beam direction of the transmitted signal, the beam direction could also have an impact on the leakage power incident on the receiver subarray. The impact of beam direction can be analyzed by evaluating the average leakage power for the receive subarray at the transmitted center frequency, $\mathbf{w}_{TX}^{H}\mathbf{S}^{H}\mathbf{S}\mathbf{w}_{TX}$, for various transmitted beam positions. Accordingly, it is worthwhile to note how the leakage isolation provided by the adaptive weights will affect the leakage power at various transmitted beam directions. The results for both uniform weights and adaptive weights are shown in Figure 4.7.

The adaptive beamforming weights were capable of reducing the leakage power for all transmitted beam positions compared to the uniform beamforming weights. There are some transmitted angles where the adaptive weights are not as effective in reducing the amount of leakage, but overall the leakage power is relatively consistent regardless of transmit beam position. For the uniformly weighted case, the highest levels of leakage are found when the array is steered toward either end of

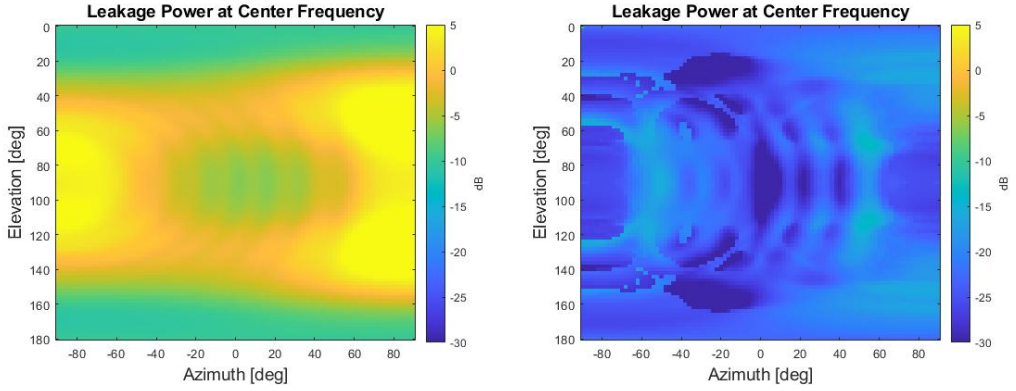

Figure 4.7: Calculated leakage power for various transmitted beam positions. Calculated with both uniform (left) and adaptive (right) transmit beamforming weights.

the array (end-fire). This result confirms intuition, as steering the beam towards the receive subarray would presumably increase the magnitude of leakage power.

4.7 Adaptive Receive Beamformer

Similar to the adaptive transmit beamformer, an adaptive receive beamformer can be designed to improve isolation between the transmit and receive subarrays by increasing SINR. Starting with the derivation of the $M \times 1$ vector of interference signals, $\mathbf{y}_{int}$, an interference covariance matrix $\mathbf{J}$ can be derived with respect to the transmitted signal interference, transmitted noise, and receiver noise at the center frequency f_0:

$$\begin{aligned}\mathbf{J} &= [\mathbf{y}_{int}^{*}\mathbf{y}_{int}^{T}] + \sigma_{RX}^{2}\mathbf{I} \\ &= P_{TX}[(\mathbf{S}\mathbf{w}_{\mathbf{TX}})^{*}(\mathbf{S}\mathbf{w}_{\mathbf{TX}})^{\mathbf{T}}] + \sigma_{\mathbf{TX}}^{\mathbf{2}}\mathbf{diag}[(\mathbf{S}\mathbf{w}_{\mathbf{TX}})^{*}(\mathbf{S}\mathbf{w}_{\mathbf{TX}})^{\mathbf{T}}] + \sigma_{\mathbf{RX}}^{\mathbf{2}}\mathbf{I}.\end{aligned} \tag{4.12}$$

Using the interference covariance matrix above, the ideal receive beamforming weights can be determined using:

$$\mathbf{w}_{rx} = k\mathbf{J}^{-\mathbf{1}}\mathbf{C}^{*} \tag{4.13}$$

where $\mathbf{C}$ is again the desired steering vector for the receive beam, and k is a scaling constant [30]. The results of the derived receive beamforming weights follow closely to the transmit beamforming weights: lower amplitudes in the column directly adjacent to the transmitting subarray, and a peak amplitude found in the center of the subarray. While the adaptive receive beamformer can be utilized to increase SINR, it is still limited by the number of saturated receive subarray elements. Any receive subarray element that is saturated will not contain usable data, and must be discarded. Because the receive beamformer is utilized in the digital domain, the

performance of the receive beamformer will be limited by the number of saturated elements after the ADC stage.

4.8 Comparison

In order to compare the benefits of utilizing adaptive transmit/receive beamformers for a multi-function array, it is helpful to define some standard metric of performance. One possible metric is to observe how the respective beamformers alter the isolation between subarrays, defined as [26]:

$$I = \frac{P_{tx}}{P_L} \tag{4.14}$$

where P_{tx} is the transmitted power from the transmitting subarray, and P_L is the leakage power incident on the receiving subarray. However, because altering the beamforming weights for the respective subarrays will affect the achievable gain, the equation for isolation must be altered slightly to compensate. Instead of comparing just the transmitted power, the equation will be modified to include the transmit gain and efficiency as well. Also, instead of just looking at the incident leakage power, the total sensitivity of the receive subarray

$$Sensitivy = \frac{P_L}{G_{rx}\epsilon_{rx}} \tag{4.15}$$

will be examined to include the reduction of receiver gain G_{rx} and efficiency ϵ_{rx} by implementation of the receive beamformers. Therefore the final definition of isolation between subarrays can be denoted as

$$I = \frac{P_{tx}G_{tx}G_{rx}\epsilon_{tx}\epsilon_{rx}}{P_L} \tag{4.16}$$

where ϵ_{tx} and G_{tx} denote the aperture efficiency and peak gain of the transmitting subarray, respectively. Therefore the isolation metric is offset by any reduction in transmitter or receiver efficiency, but increased by reductions in the incident leakage power. The isolation between subarrays for different beamforming schemes and versus element transmit power is shown in Figure 4.8.

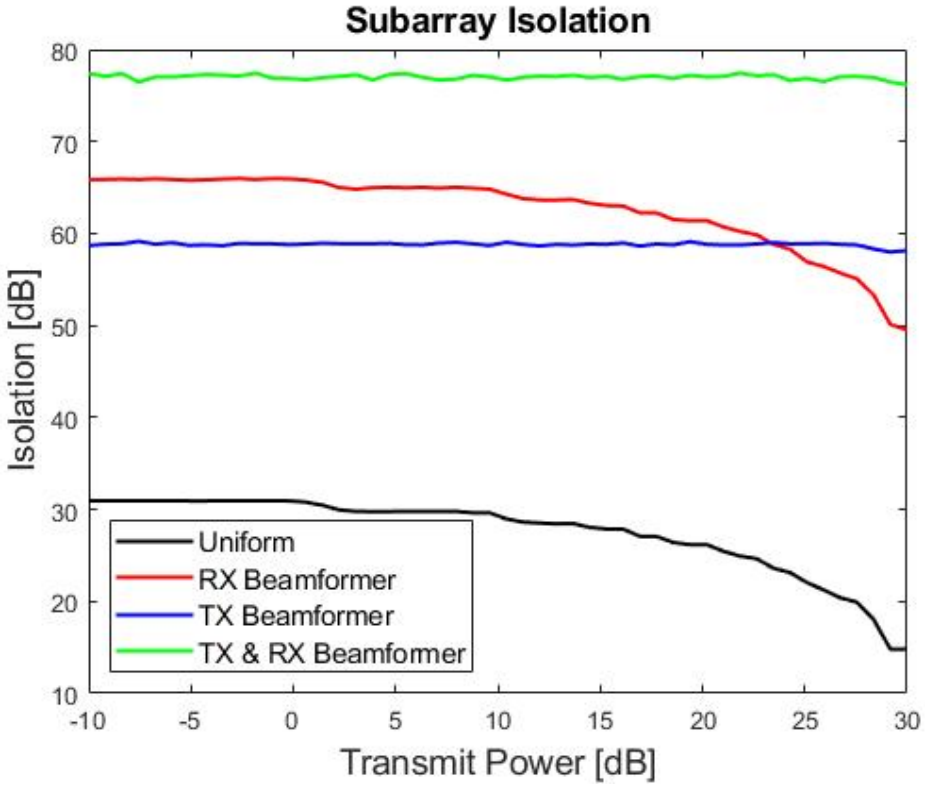

Figure 4.8: Isolation under different beamforming schemes. Transmit power is defined as power per element

The benefit of utilizing adaptive beamforming is made clear in Figure 4.8, as all adaptive beamforming schemes (on transmit and receive) provide at least a 20 dBW improvement of the isolation between subarrays. The sharp decline in isolation for the uniform and receive beamformer at high power is caused by the saturation of receiver elements, which increases as the transmit power is increased. Because the transmit beamformer reduces the number of saturated elements considerably, the

isolation does not suffer any reduction under the same transmitter power levels. Therefore there will be some level of transmitted power where the transmit beamformer will provide more isolation between subarrays than using the receive beamformer alone. Naturally, the best isolation is achieved when using both an adaptive transmit and receive beamforming scheme. If further isolation between subarrays is required, digital cancellation techniques can be implemented to remove the leakage signal directly.

Chapter 5

Digital Cancellation

Close proximity between subarrays in a partitioned aperture will inevitably lead to signals transmitted on one subarray leaking over onto the other subarrays. If all subarrays are being used to create a single beam, this leakage may not be a significant concern. However, in a multi-function scenario with multiple simultaneous beams, this leakage could be a major hindrance. Depending on the magnitude of the transmitted signals, these leakage signals could dominate the majority of the dynamic range of the adjacent subarrays. One possible solution to mitigate the leakage between subarrays is the cancellation of the leakage signal by the addition of an auxiliary signal. Cancellation of the leakage signal can be done at multiple points in the receive subarray chain, commonly split into analog and digital cancellation [31]. Analog leakage cancellation techniques have been shown to be effective at matching the coupled frequency response between elements [32]. However, in a large array, analog leakage cancellation techniques typically require increased hardware complexity and size to match the coupled response between every combination of elements. Digital leakage cancellation techniques, on the other hand, can be implemented without increases in hardware complexity [33], but the signal must be able to pass through the ADC stage of the receive subarray architecture without saturation. Otherwise, the saturated signals will distort the beamformed receive

signal beyond the capabilities of a digital cancellation scheme to match. In this study, the focus was spent entirely on digital cancellation techniques. Multiple digital cancellation techniques were implemented and compared for their effectiveness at efficiently removing the leakage signals present on the subarray. This chapter details the theory behind the digital cancellation techniques, how they are implemented in the digital system, and the limitations of digital cancellation.

5.1 Theory

Digital cancellation of the transmitted interference signal can be accomplished with the implementation of digital filters. The filters' frequency responses are set to match the frequency response of the coupling parameters outlined in Chapter 3. For complete reconstruction of the matrix $\mathbf{S}$, this approach would involve a digital filter for each individual transmit/receive element pair. Depending on the size of the array, the number of digital filters required may or may not be feasible. This system model assumes that the interference is some distortion of the initial transmitted signal, which is a valid assumption considering the leakage signal comes directly from the transmitting subarray. The interference signal on each individual receive element, $\mathbf{y_{int}}$, can be shown as the combination of interference from M transmit elements, given by:

$$y_{int}[n,t) = \sum_{m=1}^{M} s_{nm}(t) \circledast [w_{tx}[m] \odot a[m,t) + \sigma_{tx}[m,t)] \tag{5.1}$$

where $s_{nm}(t)$ is the mutual coupling channel from element m to element n, $w_{tx}[m]$ is the beamforming weight applied on element m, $\sigma_{tx}[m]$ is the transmit noise present on element m, and $a[m,t)$ is the transmitted waveform from the mth element. Because each individual transmitting element's waveform could have unique

distortions, the incident interference signal is a distorted copy of the transmitted signal from that particular element (non-ideal). Further distortions of the transmitted signal come from the individual coupling channels in $\mathbf{S}$. The received signal on each element is then the combination of the interference signal, $\mathbf{y_{int}(t)}$, any external signal of interest, $\mathbf{d(t)}$, and additive white Gaussian noise from the receive subarray, $\sigma_{rx}(t)$. The beamformed signal from N receiving elements can be then be expressed as

$$y_{rx}(t) = \mathbf{w}_{RX}^{T}(\mathbf{y}_{int}(t) + \mathbf{d}(t) + \sigma_{RX}(t)), \tag{5.2}$$

where $\mathbf{w}_{RX}$ is the length-N vector of complex receive beamforming weights. The transpose operator on the beamforming weights $\mathbf{w}_{RX}$ makes the output a scalar signal in time. In order to remove the interference signal $\mathbf{w}_{RX}^{T}\mathbf{y}_{int}$ from the beamformed receive signal, a cancellation signal y_{canc} can be added to the receive chain that is a copy of the interference signal, but 180° out of phase. y_{canc} can be constructed using a copy of the transmitted signals, $\mathbf{a}(t)$, and a FIR filter, $h_{canc}(t)$, with a frequency response set to match the frequency response of the beamformed mutual coupling channels according to

$$y_{canc}(t) = h_{canc}(t) \circledast a(t) = \mathbf{w}_{RX}^{T}\mathbf{y}_{int}(t). \tag{5.3}$$

There are many different approaches to generating the cancellation signal, two of which will be outlined here. The first involves application of the matrix $\mathbf{S}$ directly. For this approach, a separate digital FIR filter will be implemented for each individual transmit/receive pair's coupling response $s_{mn}(t)$, and then $\mathbf{w}_{RX}^{T}\mathbf{y}_{int}$ will be estimated using (5.1) and (5.2) above. The second approach generates $y_{canc}(t)$ with a single FIR filter set to equalize $\mathbf{w}_{RX}^{T}\mathbf{y}_{int}$ directly. Coefficients for the single cancellation filter can be determined using the isolated interference signal which

has been passed through the channel to be equalized and a replica of the initial transmitted waveform. The isolated interference signal can be estimated using the scattering matrix $\mathbf{S}$ from Chapter 3, or measured directly (with added noise). The filter coefficients can then be determined by minimizing the error between the isolated interference signal and the cancellation signal with a least squares approach. Up to this point, M and N have been used to describe element indices for respective subarrays. For the remainder of the digital cancellation theory, N will be used to describe the length of an FIR filter and M will be used to describe the number of time samples of the specified signal. For a N-tap cancellation filter, the interference signal and the reference transmitted signal can be constructed into two $M \times N$ matrices $\mathbf{X}$ and $\mathbf{Y}$. Each row of these matrices corresponds to M continuous time samples of the respective signals. It has been shown that the equalizer performs ideally if the number of samples is such that $M \geq 5N$ [14]. To allow the cancellation filter to perform ideally across a wide range of frequencies, a wide band calibration signal (LFM) is often used. A $N \times N$ matrix $\mathbf{H}$ of N potential vectors of length-N FIR coefficients is then used to minimize the error matrix in the least squares sense, given by

$$min\|\mathbf{E}\|^2 = min\|\mathbf{Y} - \mathbf{XH}\|^2. \tag{5.4}$$

The solution can be derived using QR decomposition of the extended signal matrix, $\mathbf{Z} = [\mathbf{X}\ \mathbf{Y}]$, constructed by appending the rows of matrix Y to the rows of matrix $\mathbf{X}$. QR decomposition of the matrix $\mathbf{Z}$ creates a unitary matrix $\mathbf{Q}$ and an upper triangular matrix $\mathbf{R}$ such that

$$\mathbf{Z}^H\mathbf{Z} = \mathbf{R}^H\mathbf{Q}^H\mathbf{QR} \tag{5.5}$$

where $\{.\}^H$ corresponds to the conjugate transpose (Hermitian) operation. Because

$\mathbf{Q}$ is a unitary matrix, the above expression can be simplified to

$$\mathbf{Z}^H\mathbf{Z} = \mathbf{R}^H\mathbf{R}. \tag{5.6}$$

The matrix $\mathbf{R}$ can be partitioned further into

$$\mathbf{R} = \begin{bmatrix} \mathbf{U} & \mathbf{V} \\ 0 & \mathbf{T} \end{bmatrix}. \tag{5.7}$$

Using the initial formulation of the signal matrix $\mathbf{Z} = [\mathbf{X}\ \mathbf{Y}]$, it can be shown that

$$\mathbf{Z^H Z} = \begin{bmatrix} \mathbf{X^H X} & \mathbf{X^H Y} \\ \mathbf{Y^H X} & \mathbf{Y^H Y} \end{bmatrix} = \begin{bmatrix} \mathbf{U^H U} & \mathbf{U}^H\mathbf{V} \\ \mathbf{V^H U} & \mathbf{V^H V} + \mathbf{T^H T} \end{bmatrix}. \tag{5.8}$$

Simplifying the upper left-hand corner,

$$\mathbf{X}^H = \mathbf{U}^H\mathbf{U}\mathbf{X}^{-1} \tag{5.9}$$

and substituting into the lower left-hand corner,

$$\begin{aligned} \mathbf{Y}^H\mathbf{X} &= \mathbf{V}^H\mathbf{U} \\ \mathbf{X}^H\mathbf{Y} &= \mathbf{U}^H\mathbf{V} \\ \mathbf{U}^H\mathbf{U}\mathbf{X}^{-1}\mathbf{Y} &= \mathbf{U}^H\mathbf{V} \\ \mathbf{Y} &= \mathbf{X}\mathbf{U}^{-1}\mathbf{V} \end{aligned} \tag{5.10}$$

the final solution given by $\mathbf{H} = \mathbf{U^{-1}V}$ can be shown. Because each column of $\mathbf{H}$ corresponds to a different filter delay, the cancellation filter delay that corresponds to the least error can be found by solving for the smallest diagonal element of $\mathbf{E^H E}$. The filter delay that produces the best performance changes in response to the different distortions applied to the transmitted waveforms, as these differences will

directly impact the interference signal incident on the array. The scattering matrix coefficients will also have a big impact on the interference signal, and as such the solution to the digital cancellation problem should be put through an analysis of its sensitivity to accurate knowledge of the scattering parameters.

5.2 System Setup

Using the two approaches for digital cancellation described above, three different system setups can be constructed. The first, shown in Figure 5.1, recreates the matrix $\mathbf{S}$ using $M \times N$ digital filters with M transmitting elements and N receiving elements. To generate the $M \times 1$ vector of input signals, the ideal waveform is replicated M times and fed into the filter's input. This approach would be effective at eliminating the leakage signal caused by $\mathbf{S}$, but could not account for any waveform distortions between transmitting elements or transmitter noise.

The second approach, shown in Figure 5.2, utilizes an observation channel on each transmitting element to measure the distorted transmitted waveform (and noise) for each transmitting element directly. The M measured waveforms are then used as the filter's input, and $\mathbf{S}$ is recreated using $M \times N$ digital filters. This approach could allow for $y_{canc}(t)$ to include all transmitted distortions and transmitter noise, and could therefore provide the optimal cancellation signal. However, observation of the transmitted signal will add more noise into the system, and the cancellation performance will now be limited by the observation noise [34]. Also, addition of the observation channels could potentially add to the complexity and size of the system, which may be undesirable.

The final approach, shown in Figure 5.3, uses a single FIR filter to create the cancellation signal from a copy of the ideally transmitted waveform. This approach

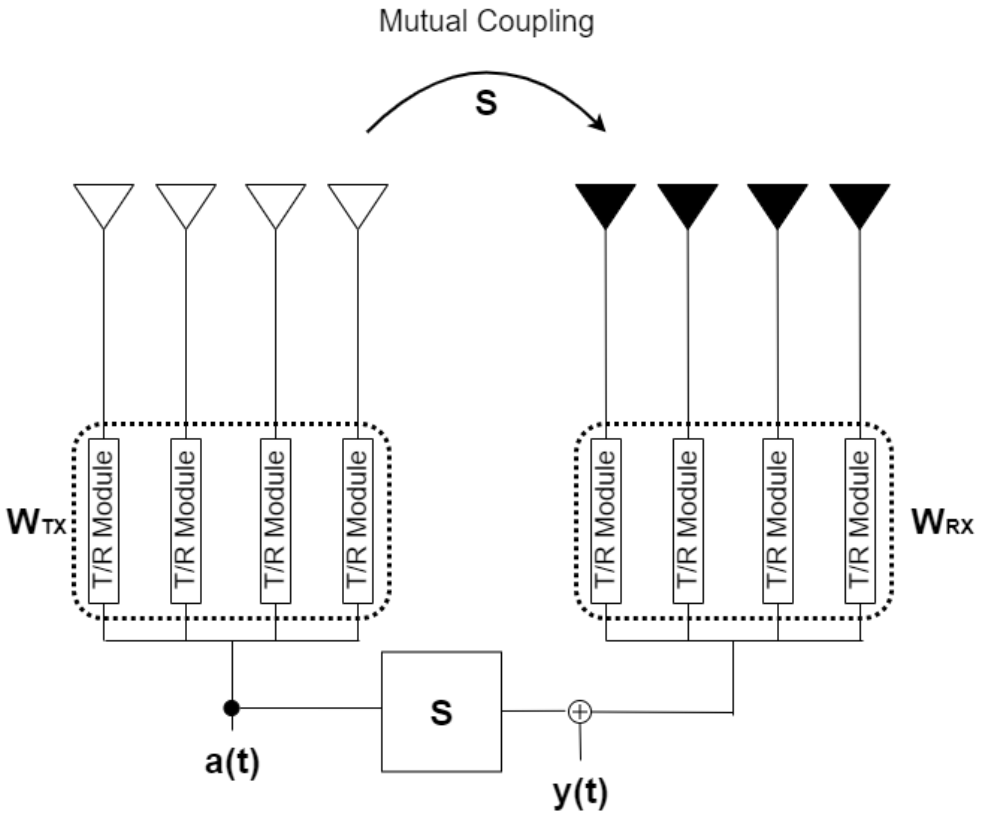

Figure 5.1: System setup utilizing complete reconstruction of S and an ideal input

must be primed with some knowledge of $y_{int}(t)$, which can be estimated using S or measured directly. While this approach will not be capable of removing the transmitter noise, it can be effective at removing the transmitted waveform distortions (assuming they are included in the priming signal $y_{int}(t)$). Depending on the sensitivity of the filter, the priming signal $y_{int}(t)$ may have to be calibrated at regular intervals. Because of the reduced complexity of this final approach, it is the main focus of this thesis, and is therefore utilized henceforth unless otherwise stated.

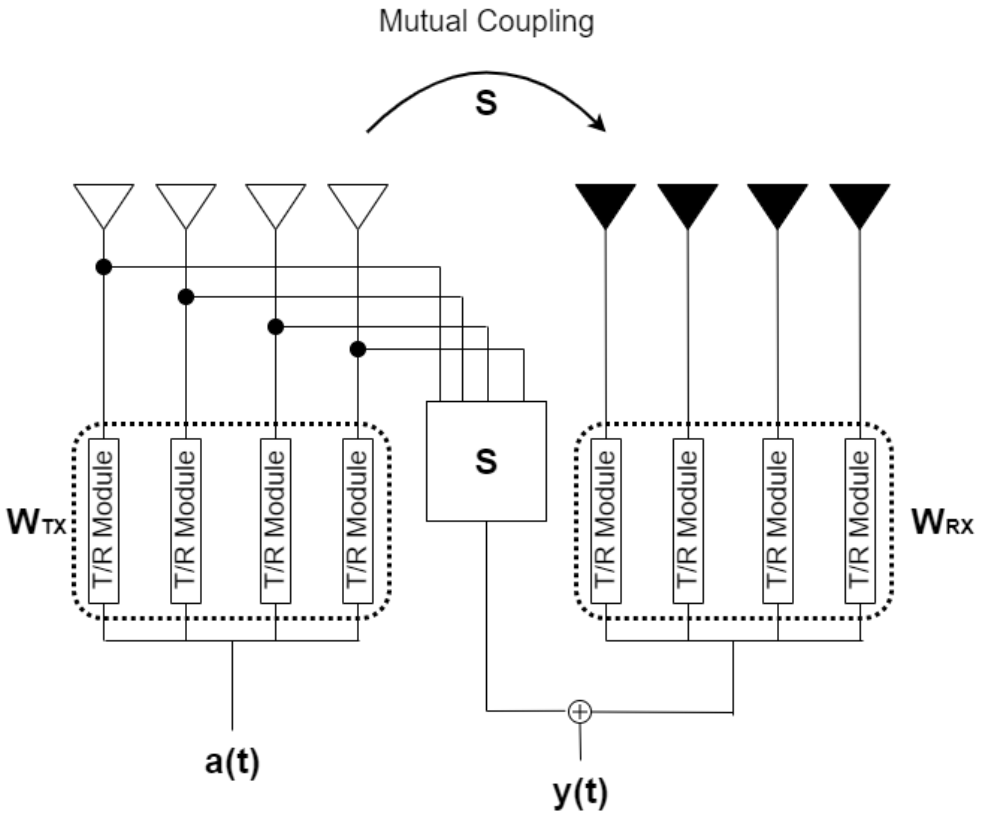

Figure 5.2: System setup utilizing complete reconstruction of S and a measured input for each transmitting element

5.3 Performance

To test the performance of the digital cancellation filter, an external 4-QAM communications signal was added incident to the receive subarray. A 100 MHz LFM waveform with a pulse time of 1 μsec was used to generate the leakage signal. Figure 5.4 shows the in-phase time domain cancellation signal, interference signal, and original waveform. The original waveform was assumed noiseless, while the interference signal had both AWGN transmitter and receiver noise. Further, it was assumed that the interference signal only contained contributions from the direct-path coupling described by the scattering parameters, as the reference cancellation

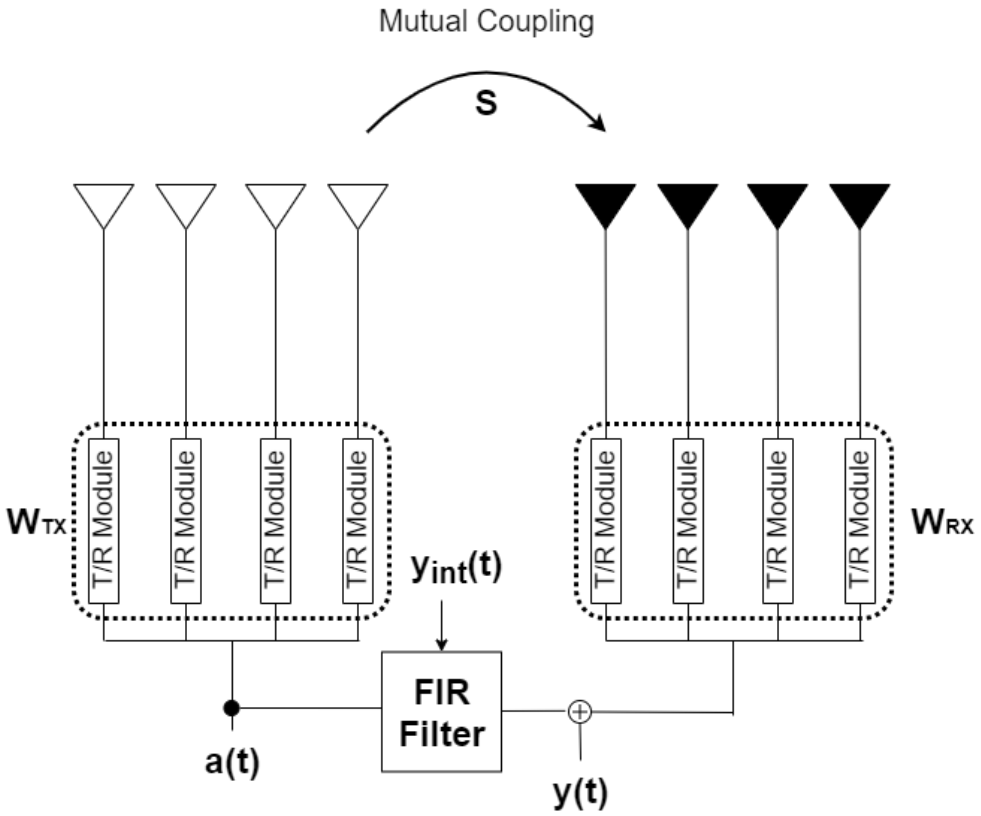

Figure 5.3: System setup utilizing a single FIR filter and a priming signal $y_{int}(t)$

signal was estimated directly from the scattering parameters. The cancellation signal does a decent job in matching the phase and amplitude of the distorted interference signal. A spectrum comparison of the distorted interference before and after the cancellation signal has been applied can be found in Figure 5.5. Clearly, the digital cancellation is effective in removing the interference signal to levels near the receiver noise floor. Without the cancellation signal, the interference signal due to transmit leakage will dominate the external QAM signal unless there is a dramatic increase in the external signal power. Also, it is important to note the spectra of the interference signal. Compared to the ideal LFM spectrum, there are noticeable distortions across frequency, caused by individual transmitter distortions and the scattering parameters $\mathbf{S}$. Because the transmitted signals have bandwidth, the com-

plexity of these distortions could be impacted by the bandwidth of the signal, which could lead to an impact on the complexity of the digital filters required.

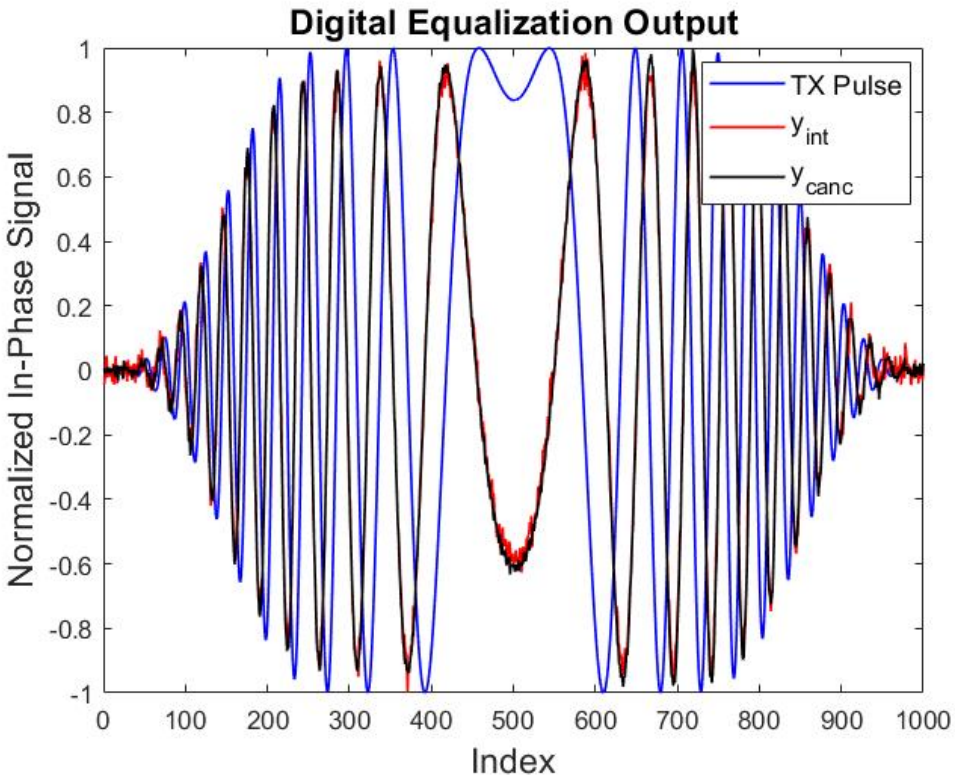

Figure 5.4: Transmitted interference signal and filtered signal

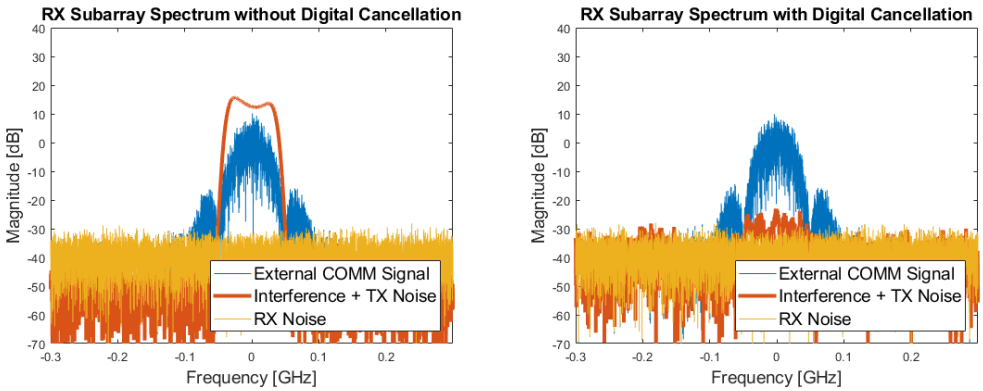

Figure 5.5: Beamformed receiver spectrum without (left) and with (right) digital cancellation

5.4 Impact of Filter Order

Traditionally, increasing the filter order on a FIR filter produces sharper responses in the frequency domain, at the expense of added complexity. Although signal distortions produced by element differences and coupling coefficients will ideally not contain any sharp transitions, increasing the filter order could allow the filter to produce a closer match to the interference signal. As such, the performance of the digital cancellation filter was compared for various filter orders. However, because the digital cancellation algorithm requires at a minimum five times the number of samples as the filter order [35], there is an upper bound on the length of the digital cancellation filter. For constant signal bandwidth, this fundamental maximum can be described in terms of the time-bandwidth product of the radar, defined as

$$TBP = \tau BW. \tag{5.11}$$

Therefore, any investigation of filter order impact on the digital cancellation filter should also include the impact of the time-bandwidth product of the radar.

To test the impact of the time-bandwidth product on the digital cancellation algorithm, the same 16×16 array used previously was implemented with various transmitted waveforms containing different time-bandwidth products. The average residue leakage power after digital cancellation is shown in Figure 5.6 versus filter order for various time-bandwidth product values of a LFM pulse. To generate different time-bandwidth products, the pulse time of the radar was kept at a constant 1 μs and the bandwidth of the signals varied from 10 MHz to 250 MHz. Also shown on the figure is the $M \geq 5N$ point, where any filter order larger than this limit will not have enough samples for good solutions. This degradation of filter perfor-

mance can be easily seen in Figure 5.6, as the residue power starts to increase again when $M \leq 5N$. The time-bandwidth product also has an effect on the residue power. Because the coupling parameters estimated in Chapter 3 were relatively smooth throughout the bandwidth of the waveform, the filter required to generate the cancellation signal is a low-order filter. However, higher time-bandwidth products require slightly higher filter orders to achieve optimal performance, and tend to leave behind higher levels of residue power for lower filter orders. This result is only evident for low filter orders (N = 1-3), but would be expected to become more evident as the complexity of the coupling channel's frequency response is increased.

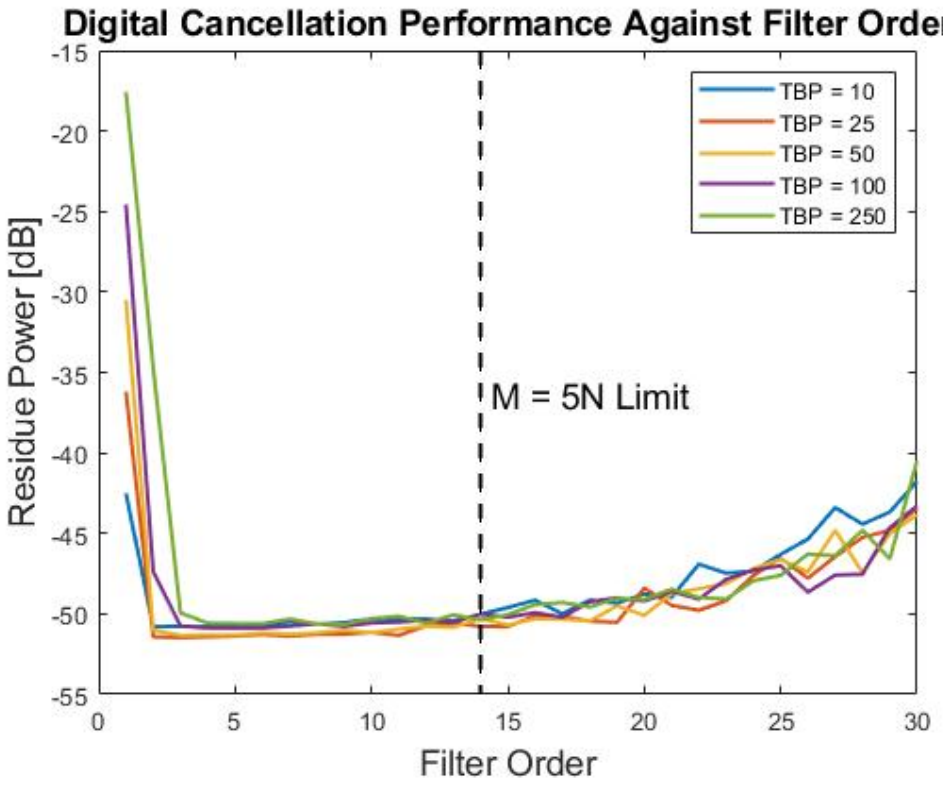

Figure 5.6: Residue power after digital cancellation versus filter order for different time-bandwidth products

5.5 Impact of Transmitter Noise

The digital cancellation algorithm depends on the ability to distinguish the interference signal from the surrounding transmit and receive noise. Because of the close proximity between subarrays, the leakage signal power will typically be much higher than the receiver noise floor, and receiver noise will not significantly impact the interference estimate. However, as the interference signal comes directly from the transmitted signals, the transmitter noise levels could impose a limit on the performance of the digital cancellation. This limit would impact the dynamic range of the receiver, which would now have a minimum limit set by either the coupled transmitter noise level or the receiver noise level after ideal cancellation. Therefore the transmitter noise level is an important factor to examine when evaluating the performance of digital cancellation algorithms.

To examine the impact of transmitter noise on digital cancellation, the performance of the digital cancellation filter was implemented under different transmitter noise levels. Using the same 16×16 array with two subarrays shown previously, the transmitted waveforms were kept at a constant -10 dBW per element while the transmitter noise level varied. Figure 5.7 shows the residue power after digital cancellation of the leakage signal under differing levels of transmitter noise power, for each of the three discussed techniques. When the transmitter noise power is below -100 dBW, the receiver noise after cancellation dominates and the residue power remains constant for both the single FIR filter and the measured waveform methods. However, as the transmitter noise level is increased, the residue power has a proportional increase for the single FIR filter technique, but not for the technique of directly measuring the transmitted signals. This confirms that measuring the transmitted signals directly for each transmitted pulse will allow the cancellation signal

to include any transmitter noise, at the cost of increased complexity. For the single FIR filter technique, the transmitter noise dominates and the digital cancellation signal is only capable of limiting the leakage to the transmitter noise level. The method of recreating the cancellation signal using only ideal waveforms has the highest levels of leakage residue, as it does not recreate any transmitter distortions or transmitter noise.

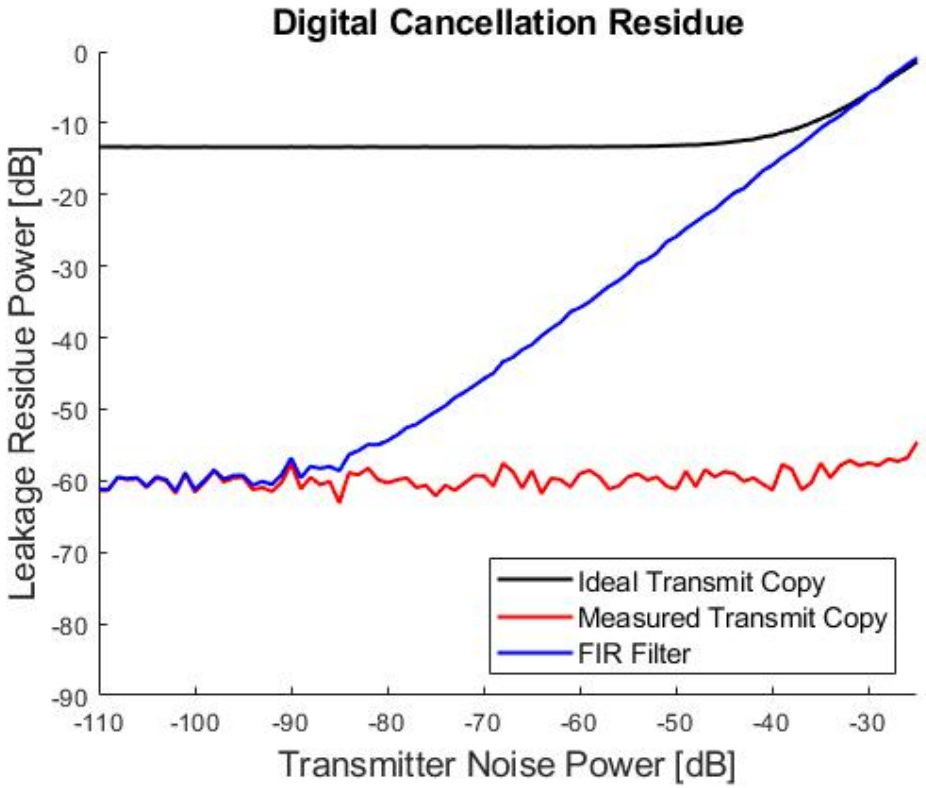

Figure 5.7: Residue power after digital cancellation as a function of transmitter noise level for each of the three proposed techniques. The single FIR filter technique is denoted as FIR filter, while the other techniques are denoted with respect to the system inputs.

5.6 Sensitivity to Mutual Coupling Estimation

Just as in the case with the adaptive beamformer, the digital cancellation algorithm can derive its solution directly from the scattering parameters. However, as there will always be some level of uncertainty in the measured scattering parameters, the accuracy of the scattering parameter measurements will have an effect on the digital cancellation performance. To test the sensitivity to the scattering parameters, the performance of the digital cancellation technique was tested for various levels of uncertainty added into the scattering parameters, with the transmitting subarray transmitting -10 dBW per element with a transmitter noise level of -100 dBW. The reduced signal power was done to ensure that all receive subarray elements were below saturation, so that only the effectiveness of the digital cancellation algorithm would be compared. Figure 5.8 plots the residue power of the digital cancellation in the absence of any external signals. For reference, the leakage power without any digital cancellation was also shown. Normally distributed error was added into the scattering parameters to match the magnitude of both the real and imaginary portions of the scattering matrix coefficients, with a standard deviation set to some percentage of the original coefficients. Multiple trials were simulated for each noise distribution, and the average performance of each was shown in Figure 5.8.

Looking at Figure 5.8, the best performance is obviously found when knowledge of the scattering matrix is 100% accurate. However, the performance decreased dramatically as the interference power is increased. While there is still some benefit to adding the digital cancellation signal even with high levels of uncertainty in $\mathbf{S}$, the performance declines much more rapidly than the performance of the adaptive beamformer discussed in Chapter 4.

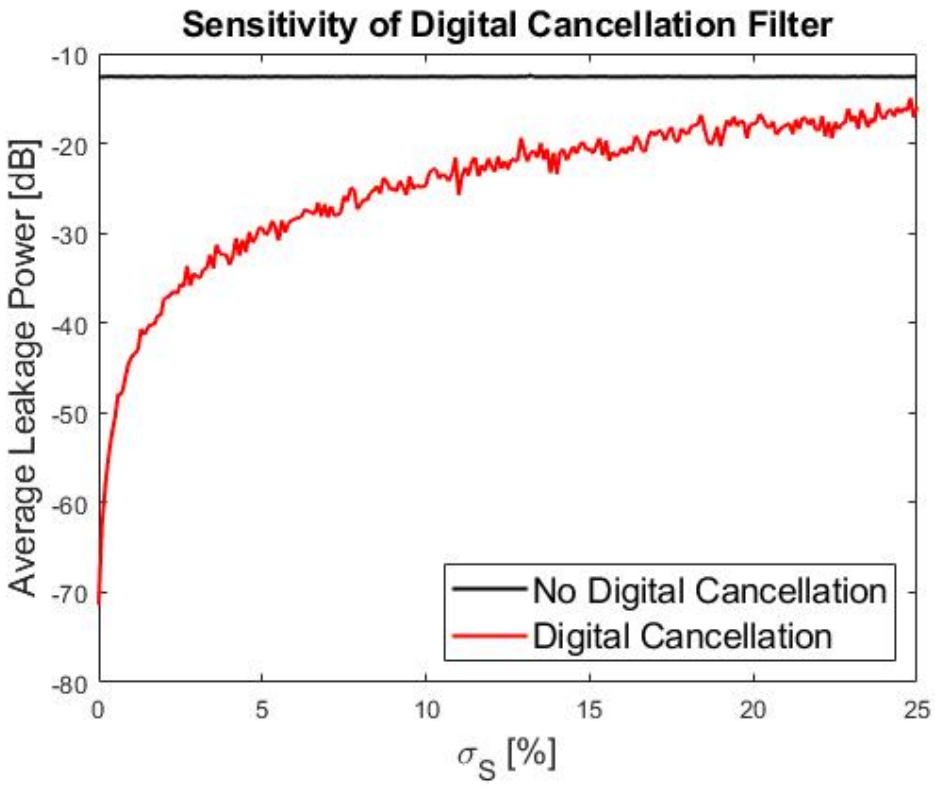

Figure 5.8: Residue power as a function of uncertainties in the S-matrix

Other configurations of digital cancellation attempt to measure the leakage signals directly by isolating the leakage signal on the receivers, and then determining the coupling channel response needed to recreate the leakage signal from a stored copy of the transmitted waveform [26]. Even though this method measures $y_{int}(t)$ directly instead of deriving it from the measured scattering parameters, the performance of the digital cancellation filter would still be sensitive to the ability to accurately measure $y_{int}(t)$. Therefore, whether the interference signal $y_{int}(t)$ is measured directly or estimated from measured $\mathbf{S}$ parameters, the same sensitivity trend would be expected.

Chapter 6

Results

In our application, the performance of a multi-function array performing aperture-level STAR can be defined by its ability to decode external signals, uninterrupted by the radar transmission. Implementation of adaptive beamforming and/or digital cancellation can be shown to improve the performance of the multi-function array by increasing the dynamic range of the receivers, subtracting leakage signals from the beamformed signal, and increasing the isolation between subarrays. This chapter provides additional analysis of how each of the algorithms impact the total multi-function performance of the array by examining the ability of the receive subarray to decode external QAM communication signals.

6.1 Simulation Setup

All results presented in this section were calculated for a simulated 16×16 array, split vertical into two equally sized subarrays. One subarray was transmitting 100 MHz LFM signals with a pulse time of 1 μsec, directed broadside to the array. The other subarray was dedicated to receiving an external N-QAM signal, incident 10° off azimuth. The BER of the external QAM signal was calculated to compare the performance of both the adaptive beamforming and digital cancellation

algorithms. Because the primary concern of STAR is the ability to receive signals during transmission, the BER was only calculated during periods when the radar was transmitting pulses.

6.2 Adaptive Beamforming

The first algorithm tested was adaptive beamforming. The biggest impact adaptive beamforming had on the multi-function performance of the array was the impact on the dynamic range. The lower end of the dynamic range of the receiver will always be set by either the coupled leakage signals or the receiver noise floor. Because radars typically require high-power transmitters, the coupled leakage signals will usually dominate, and can even be strong enough to push individual receivers to saturation. The adaptive transmit beamforming techniques discussed in Chapter 4 reduce the leakage power incident on the array by altering the transmit weights. Figure 6.1 shows the dynamic range improvement that can be achieved on each receive subarray element using the derived adaptive beamforming weights. The blue regions of the plot indicate the original dynamic range of the receivers, while the red regions indicate the leakage signal levels. Saturation has already been shown to dramatically reduce performance, and any elements that are completely saturated must be discarded. For non-saturated elements, the dynamic range will have a minimum limit set by the leakage signal amplitude. Any external signal level below the leakage signal limit will be masked and require additional signal processing techniques to decode. By applying the adaptive transmit weights, the leakage signal levels were reduced by about 30 dBW for the most adjacent receiver elements, and drops many elements out of saturation. The leakage level still dominates the majority of the dynamic range, but the application of the adaptive weights improves the

data quality and can increase the overall SINR for constant signal levels.

Correspondingly, increasing the dynamic range has a significant impact on the performance of the array to decode the external signals. By reducing the number of saturated elements, the adaptive beamforming weights could provide enough subarray isolation to enable STAR without any additional mitigation techniques, depending on the system setup. If further isolation between subarrays is required, the use of digital cancellation techniques may be necessary.

6.3 Digital Cancellation

This section discusses the performance of the digital cancellation algorithm. Digital cancellation of the leakage signals can provide an increase in the SINR of the receiver by eliminating the leakage interference directly. As discussed earlier, without digital cancellation, the dynamic range of the system is limited by the interference leakage signal. The performance of the digital cancellation is limited by the transmitter noise and the accuracy of the coupling channel model. For the results listed in this section, the transmit subarray was transmitting pulses at 1 W

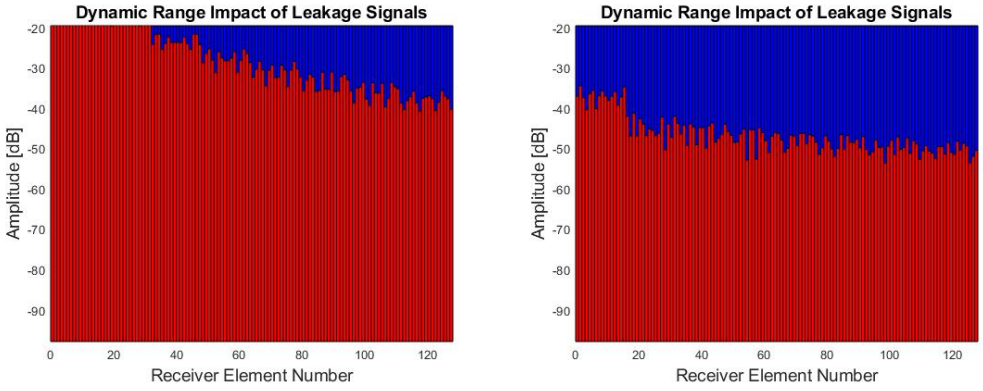

Figure 6.1: Dynamic range of receiver elements with incident leakage signal, without (left) and with (right) adaptive beamforming. Blue regions indicate the original dynamic range of the receiver, and the red regions indicate the leakage signal levels.

per element with a uniform transmit beamformer, producing leakage signals that dominated the external QAM signals. Then, the signal quality was examined with and without the implementation of the digital cancellation algorithm.

One common technique to visualize signal quality is to generate the signal constellations. These constellations are sampled directly at the sampling rate of the signal, and should therefore be relatively uniformly spaced and tightly grouped for high quality signals. If the signal quality is low, the constellation will be erratic. Figure 6.2 shows the beamformed signal constellations of an external 16-QAM signal, with and without digital cancellation. Clearly, the signal constellations without digital cancellation are difficult to decipher when the interference power dominates, as the symbols do not seem to match any accepted symbol region. The main issue seen is that the interference signal amplitude is too large, dominating the 16-QAM signal. However, in-between transmitter pulses, the receiver is able to decode the symbols. With the added digital cancellation signal, the system is now able to decode the symbols during and after the transmitted pulses. However, during the radar pulse transmission, the performance is slightly degraded compared to the baseline

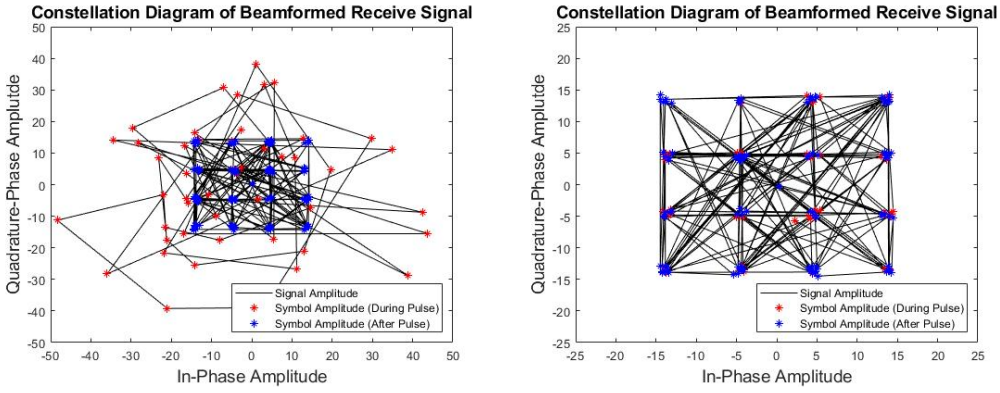

Figure 6.2: Constellation diagrams of beamformed receive signal with (right) and without (left) added digital cancellation signal. The view of the right diagram was zoomed in to highlight the difference in symbol variance during and after radar pulse transmission

case. This is evident by the spread of the symbols during radar transmission on the constellation compared to the spread of the symbols measured after transmission. This performance degradation comes from imperfections in the digital cancellation signal and the inability of the cancellation signal to remove all transmitter noise present on the receive subarray.

Another limiting factor on the performance of the digital cancellation is the transmitter noise level. Even if the digital cancellation is ideal, there will still be some transmitter noise attached to the leakage signal that will be difficult to remove. If this transmitter noise level is significant, the SNR of the external signal will be degraded and potentially impossible to decode. A good technique to examine the noise impact is to generate eye diagrams of the QAM signal. Eye diagrams are generated by over-sampling the external signal during the transition between symbols, and overlaying the results for each symbol period. Figure 6.3 shows eye diagrams of an external 4-QAM signal under differing levels of transmitter noise. For comparison, the eye diagrams also include the signals recorded without any incident leakage noise or waveforms (in-between pulses).

Looking at Figure 6.3, it is clear that the transmitter noise level can impact the data quality of the external signal significantly. Compared to regions in between pulses, the signals during transmission have noticeable deviations caused by the impact of transmitter noise. These deviations increase dramatically with increases in the transmitter noise level, and could potentially lead to symbol errors. The transmitter noise level is therefore the minimum residue achievable after ideal digital cancellation, and must be considered when analyzing the STAR capability of the system. However, because the leakage transmitter noise level also passes through the coupling channels derived in Chapter 3, the use of beamforming techniques can be utilized to limit the leakage transmitter noise level present. Therefore it is ex-

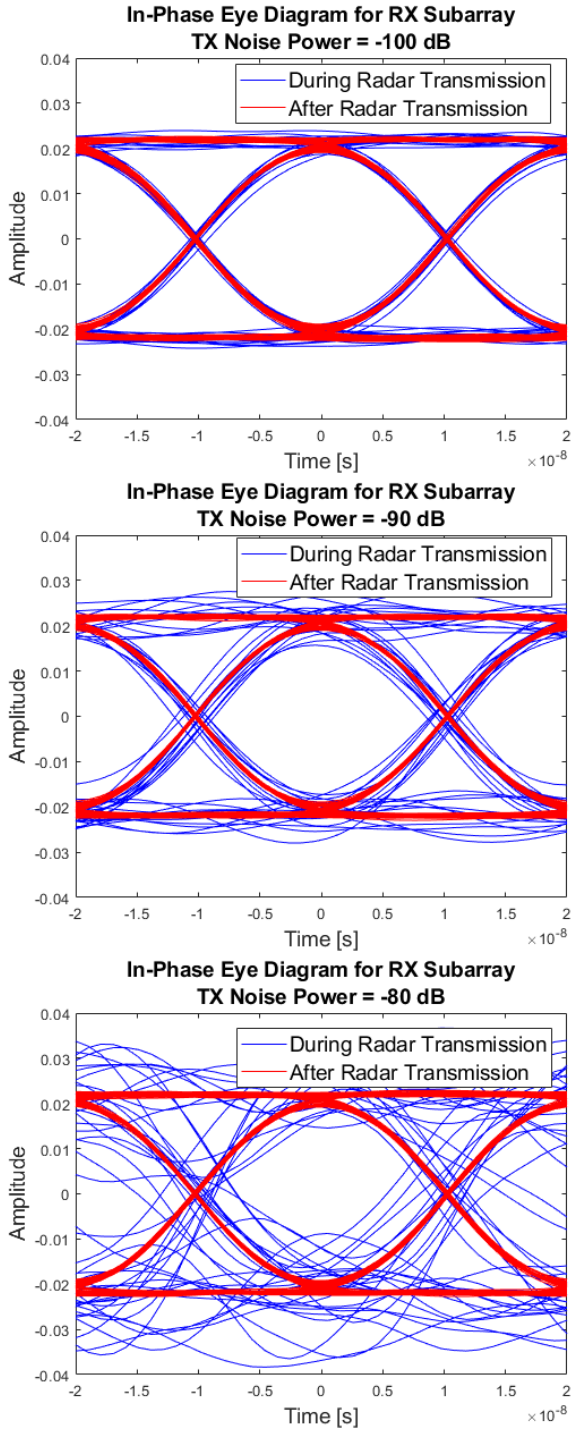

Figure 6.3: Eye diagrams of beamformed 4-QAM signal under differing levels of transmitter noise. Plotted during and after transmitted radar pulse.

pected that a combination of adaptive beamforming and digital cancellation would have the best performance towards STAR capability.

6.4 Total

By utilizing a combination of adaptive beamforming and digital cancellation, the optimal multi-function performance of the array can be achieved. To test the performance, bit-error rates (BER) were compared under various conditions: with and without adaptive beamforming weights, and at different transmitter power levels. The digital cancellation technique discussed in Chapter 5 was also implemented for all tests. Figure 6.4 shows the results. As expected, the adaptive weights provided better BER than uniform weights for every transmitter power level. Recall from Chapter 4 that this performance comes at the cost of transmitter gain. However, as the transmitter power level is increased, the performance of the adaptive weights becomes even better compared to the corresponding uniform weights. This can be seen by comparing the external signal power levels required for the same BER; When transmitting with 1 W per element, the adaptive transmitter weights enable the same BER with 5 Watts less external signal power, 10 Watts less when the array is transmitting 10 Watts per element, and 525 Watts less when the array is transmitting 100 W per element. The case where the array was transmitting 100 Watts per element has high oscillations caused by the increasing number of saturated elements as the external signal power is increased. The combination of the high transmitter leakage power and the power levels of the external signal required for decoding leads to an increase in the number of saturated elements not seen in any other case. While transmitting 100 Watts per element in an array might seem unreasonable, it is worth mentioning again that the BER behaviour would be highly

dependent on the ADC stage. Reduction in the number of bits or an increased sensitivity will degrade the BER performance by lowering the saturation limit of each receive subarray element, thereby increasing the total number of saturated receive subarray elements. The adaptive transmit weights will be beneficial regardless, because the adaptive weights have already been shown to be effective at reducing the number of saturated elements for any transmit power level compared to uniform weighting.

The isolation between subarrays, defined in Chapter 4, provides the best comparison for the effectiveness of the various algorithms. Figure 6.5 shows the isolation provided for different array schemes and transmitter power levels. Without digital cancellation, the isolation provided by a combination of adaptive transmit

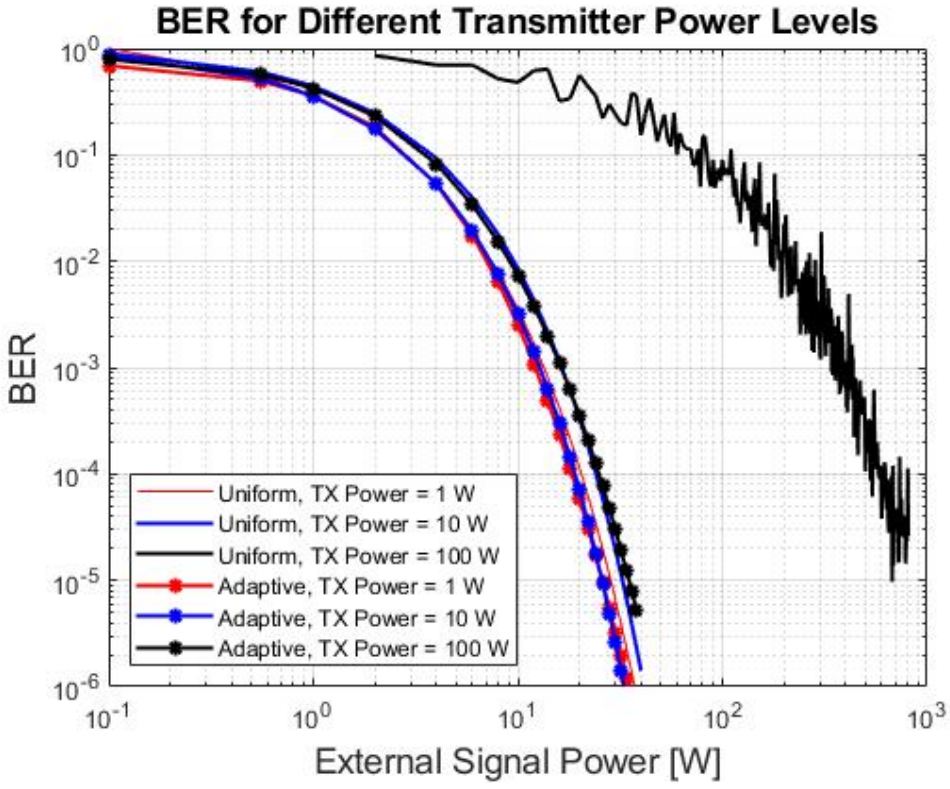

Figure 6.4: Bit-error rates for different transmit beamforming schemes and transmitter power levels

and receive beamformers is significantly higher than the uniform case. The isolation improvement is especially prevalent as the transmitter power levels are increased. If only a transmit or a receive beamformer is utilized, the best isolation performance depends on the transmitter power levels. This is a result of the receive subarray elements becoming saturated, which minimizes the performance of the receive beamformer. The transmit beamformer, on the other hand, reduces the number of saturated elements while maintaining a constant loss of transmitter gain. Without utilizing any adaptive beamformers, the isolation is significantly reduced. Depending on the parameters of the system, adaptive beamforming alone might be capable of providing STAR functionality. Otherwise, further isolation can be provided by implementation of digital cancellation.

By utilizing digital cancellation of the leakage signal along with the adaptive beamformers, the isolation between subarrays is maximized. However, the isolation improvement by utilizing adaptive beamformers on top of the digital cancellation is minimal. The isolation does increase slightly with adaptive beamformers at higher transmitter power levels, but overall the performance is pretty constant. Ideally, the digital cancellation would reduce the leakage power down to the transmitter noise floor, and any beamforming schemes would only affect the transmitted noise. Therefore, for higher levels of transmitter noise, adaptive beamforming might provide additional benefits even after digital cancellation by reducing the coupled noise level.

To ensure that improving the isolation between subarrays would have a corresponding improvement in the BERs of the array, the BER was calculated for an external 16-QAM signal while the array was utilizing combinations of all of the STAR techniques mentioned above. The results are shown in Figure 6.6. The results in Figure 6.6 mirror the results shown in Figure 6.5. Substantial benefits to the

BER can be provided by adaptive beamforming, with further benefits provided by digital cancellation. The results in Figure 6.6 show that STAR can be accomplished by a partitioned aperture, and that the performance can be improved by utilization of the algorithms shown in this thesis.

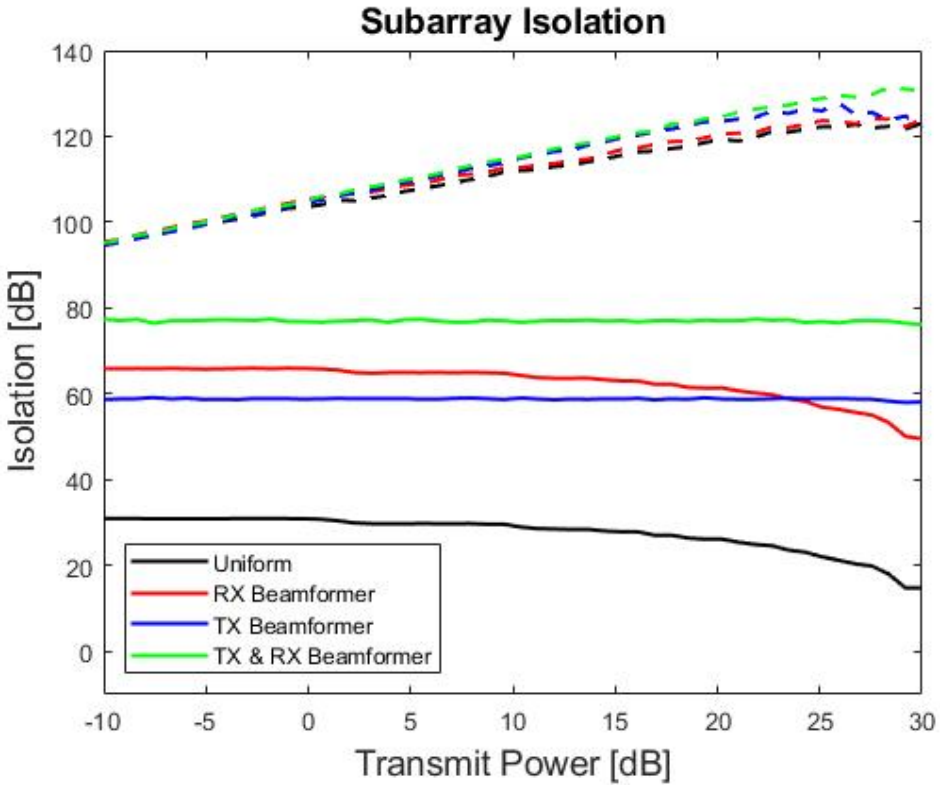

Figure 6.5: Subarray isolation provided by STAR algorithms. Dotted lines indicate digital cancellation of the transmitted leakage signals

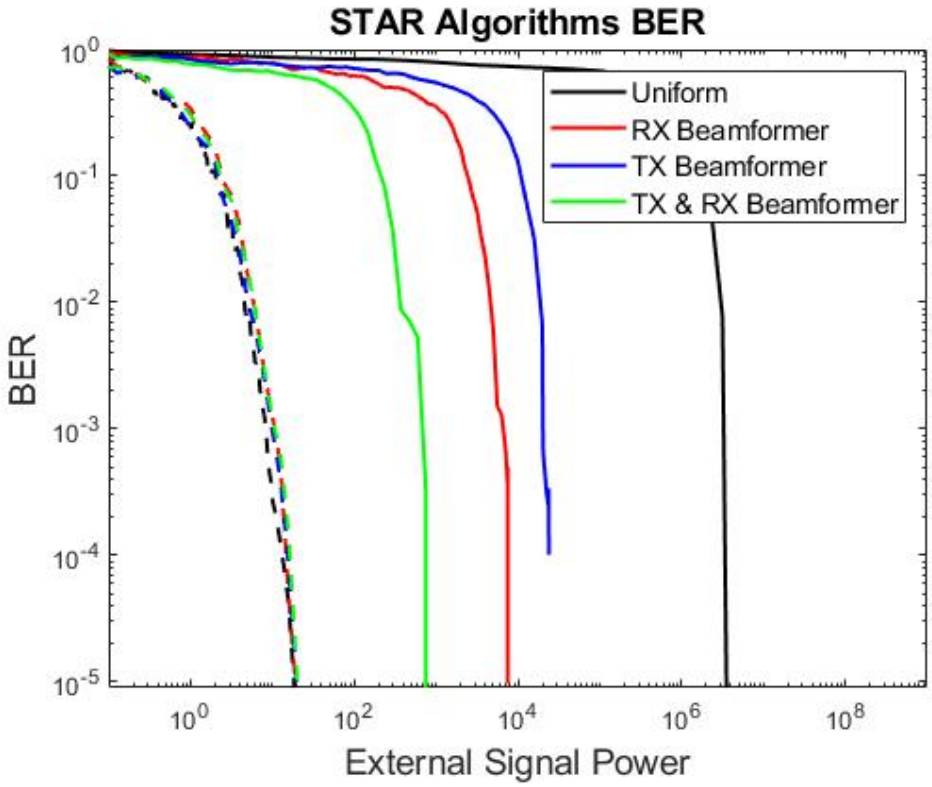

Figure 6.6: Bit-error rates of the external signal provided by STAR algorithms. Dotted lines indicate digital cancellation of the transmitted leakage signals. Signal power is referenced from transmitting antenna 10 km from array.

Chapter 7

Conclusion & Future Work

This thesis has explored how aperture-level STAR can be implemented with an all-digital array, detailed the limitations provided by mutual coupling in the array, and provided techniques for improving the isolation between transmit/receive subarrays. The advantages and flexibility provided by aperture-level STAR have been discussed, with isolation between subarrays proving to be the largest hindrance toward ideal performance. Because the mutual coupling between subarrays produces the biggest detriment toward subarray isolation, a good understanding of the mutual coupling parameters can be utilized in conjunction with digital algorithms to increase subarray isolation. Adaptive beamforming on both transmit and receive beams has been shown to be effective at increasing subarray isolation, without significant impact on the transmitted beams. Digital cancellation of the distorted transmitted interference provides the highest levels of isolation, but can be limited by transmitter dynamic range and channel knowledge of the mutual coupling parameters. Different architectures for digital cancellation can reduce the leakage power even further to levels below the transmitter noise floor, at the cost of higher complexity in the system. Combinations of beamforming and digital cancellation provide the highest levels of isolation, and can be dynamically utilized in an all-

digital array to match system requirements for STAR.

Multiple algorithms for aperture-level STAR have been detailed in this thesis, but opportunities for research still abound. Dynamic aperture reconfiguration can be utilized to maximize the efficiency of the array and tailor the subarray configuration to the desired system needs. Trade-offs between transmitter/receiver gain and isolation requirements produce interesting avenues for further research into dynamic array systems. While this thesis sought to use adaptive beamforming to improve the isolation between subarrays as much as possible, separate constraints can be imposed to reduce the leakage power just below the saturation limit and maintain as much transmit gain as possible. With continuous advancements and flexibility in radar waveform design in digital arrays, digital cancellation of transmitted interference must become ubiquitous against all transmit schemes. Improvements in noise radar technology will allow for non-correlated self-interference, which will improve the subarray isolation even further after beamforming. Also, hardware imperfections and limitations will provide unique obstacles for the digital cancellation architecture to handle. One possible example includes non-linear effects from high-power amplification on transmitted signals that will require more precise matching networks for effective digital cancellation. While this thesis has explored the foundations of aperture-level STAR in digital arrays, further research and testing of digital array systems will illuminate exciting new areas to explore in STAR systems.

References

[1] E. Brookner, "Recent developments and future trends in phased arrays," *IEEE Int. Symp. Phased Array Syst. Technol.*, pp. 43–53, 2013.

[2] J. M. Loomis, "Army radar requirements for the 21st century," in *2007 IEEE Radar Conference*, 2007, pp. 1–6.

[3] S. H. Talisa, K. W. O'Haver, T. M. Comberiate, M. D. Sharp, and O. F. Somerlock, "Benefits of digital phased array radars," *Proceedings of the IEEE*, vol. 104, no. 3, pp. 530–543, 2016.

[4] C. A. Recknagel and N. A. Goodman, "Simulation and adaptive sub-array packing for an all-digital phased-array radar," in *2019 IEEE Radar Conference (RadarConf)*, 2019, pp. 1–6.

[5] A. T. Wegener and W. J. Chappell, "High isolation in antenna arrays for simultaneous transmit and receive," in *2013 IEEE International Symposium on Phased Array Systems and Technology*, 2013, pp. 593–597.

[6] G. Barb, M. Otesteanu, F. Alexa, and A. Ghiulai, "Digital beamforming techniques for future communications systems," in *2020 12th International Symposium on Communication Systems, Networks and Digital Signal Processing (CSNDSP)*, 2020, pp. 1–4.

[7] M. Agrawal and S. Prasad, "Robust adaptive beamforming for wide-band, moving, and coherent jammers via uniform linear arrays," *IEEE Transactions on Antennas and Propagation*, vol. 47, no. 8, pp. 1267–1275, 1999.

[8] K. E. Kolodziej, B. T. Perry, and J. S. Herd, "Simultaneous transmit and receive (star) system architecture using multiple analog cancellation layers," in *2015 IEEE MTT-S International Microwave Symposium*, 2015, pp. 1–4.

[9] K. L. Scherer, S. J. Watt, E. A. Alwan, A. A. Akhiyat, B. Dupaix, W. Khalil, and J. L. Volakis, "Simultaneous transmit and receive system architecture with four stages of cancellation," in *2015 IEEE International Symposium on Antennas and Propagation USNC/URSI National Radio Science Meeting*, 2015, pp. 520–521.

[10] S. Huberman and T. Le-Ngoc, "Mimo full-duplex precoding: A joint beamforming and self-interference cancellation structure," *IEEE Transactions on Wireless Communications*, vol. 14, no. 4, pp. 2205–2217, 2015.

[11] C. Fulton, M. Yeary, D. Thompson, J. Lake, and A. Mitchell, "Digital phased arrays: Challenges and opportunities," *Proceedings of the IEEE*, vol. 104, no. 3, pp. 487–503, 2016.

[12] R. M. Davis and R. L. Fante, "A maximum-likelihood beamspace processor for improved search and track," *IEEE Transactions on Antennas and Propagation*, vol. 49, no. 7, pp. 1043–1053, 2001.

[13] E. I. Ackerman, C. H. Cox, H. V. Roussell, and P. S. Devgan, "Broadband simultaneous transmit and receive from a single antenna using improved photonic architecture," in *2019 IEEE MTT-S International Microwave Symposium (IMS)*, 2019, pp. 778–781.

[14] J. Lake, M. Yeary, and R. Palmer, "Real-time digital equalization to enhance element-level digital beamforming," in *2019 IEEE Radar Conference (RadarConf)*, 2019, pp. 1–6.

[15] M. I. Skolnik, *Introduction to Radar Systems*, 2nd ed. McGraw-Hill, 1980.

[16] F. G. Stremler, *Introduction to Communication Systems*, 3rd ed. Addison-Wesley Publishing Co., 1990.

[17] D. F. Kelley and W. L. Stutzman, "Array antenna pattern modeling methods that include mutual coupling effects," *IEEE Transactions on Antennas and Propagation*, vol. 41, no. 12, pp. 1625–1632, 1993.

[18] H. Wang, D. G. Fang, Y. P. Xi, C. Z. Luan, and B. Wang, "On the mutual coupling of the finite microstrip antenna arrays," in *2007 International Symposium on Electromagnetic Compatibility*, 2007, pp. 10–14.

[19] S. Henault and Y. M. M. Antar, "Accurate evaluation of mutual coupling for array calibration," in *2009 Computational Electromagnetics International Workshop*, 2009, pp. 34–37.

[20] N. Peccarelli and C. Fulton, "A mutual coupling approach to digital predistortion and nonlinear equalization calibration for digital arrays," in *2019 IEEE International Symposium on Phased Array System Technology (PAST)*, 2019, pp. 1–8.

[21] D. M. Pozar, *Microwave engineering; 3rd ed.* Hoboken, NJ: Wiley", 2005".

[22] J. S. Herd and H. Steyskal, "Multipath scattering compensation for low sidelobe pattern synthesis on a complex platform," in *Proceedings, IEEE Aerospace Conference*, vol. 2, 2002, pp. 2–2.

[23] C. A. Balanis, *Advance Engineering Electromagnetics*, 1st ed. John Wiley, 1989.

[24] ——, *Antenna Theory: Analysis and Design*, 3rd ed. John Wiley, 2005.

[25] A. B. Gershman, U. Nickel, and J. F. Bohme, "Adaptive beamforming algorithms with robustness against jammer motion," *IEEE Transactions on Signal Processing*, vol. 45, no. 7, pp. 1878–1885, 1997.

[26] J. P. Doane, K. E. Kolodziej, and B. T. Perry, "Simultaneous transmit and receive with digital phased arrays," in *2016 IEEE International Symposium on Phased Array Systems and Technology (PAST)*, 2016, pp. 1–6.

[27] D. Sweet, "Performance of stochastic gradient descent adaptive beamforming using sonar data," in *IEE Proceedings H (Microwaves, Optics, and Antennas)*, vol. 130, no. 1, 1983, pp. 147–151.

[28] S. Haykin, *Adaptive Filter Theory*, 4th ed. Prentice Hall, 2002.

[29] D. H. Johnson and D. E. Dudgeon, *Array Signal Processing: Concepts and Techniques*, 1st ed. Prentice Hall, Inc., 1993.

[30] M. Richards, *Fundamentals Of Radar Signal Processing*. McGraw-Hill Education (India) Pvt Limited, 2005. [Online]. Available: https://books.google.com/books?id=qizdSv8MEngC

[31] E. Ahmed and A. M. Eltawil, "All-digital self-interference cancellation technique for full-duplex systems," *IEEE Transactions on Wireless Communications*, vol. 14, no. 7, pp. 3519–3532, 2015.

[32] S. J. Watt, E. A. Alwan, and J. L. Volakis, "Cascaded network analysis of a wideband rf self-interference cancellation (rf-sic) filter for star systems," in *2016 IEEE International Symposium on Antennas and Propagation (APSURSI)*, 2016, pp. 2117–2118.

[33] I. T. Cummings, J. P. Doane, T. J. Schulz, and T. C. Havens, "Aperture-level simultaneous transmit and receive with digital phased arrays," *IEEE Transactions on Signal Processing*, vol. 68, pp. 1243–1258, 2020.

[34] T. He, W. Shen, and H. Li, "Aperture-level simultaneous transmission and reception based on digital cancellation in radar system," in *2019 International Radar Conference (RADAR)*, 2019, pp. 1–4.

[35] J. R. Johnson, A. J. Fenn, H. M. Aumann, and F. G. Willwerth, "An experimental adaptive nulling receiver utilizing the sample matrix inversion algorithm with channel equalization," *IEEE Transactions on Microwave Theory and Techniques*, vol. 39, no. 5, pp. 798–808, 1991.